



Comprehensive Analysis of Nitrogen–Oxygen Schiff Base Derived from Triazole and Its Metal Complex: Synthesis, Structural Characterization, and Biological Activities with Theoretical Insights for Anti-*Helicobacter pylori*, Antitumor, and Anti-COVID-19 Applications

Shimaa el gazar*, Abeer Taha Ibrahim, Walaa H. Mahmoud, Ahmed A. El-Sherif



Chemistry Department, Faculty of Science, Cairo University, Giza, 12613 Egypt

Abstract

The current experiment aims to lay bare the transition metal compounds that feature the Schiff base Complex Ligand ((E)-(2-(2-(1-(1H-benzotriazol-1-yl)propan-2-ylidene)hydrazineyl)-2-oxoacetamide)(also referred to as (L))). Such results could be observed: these investigations were relatively prosperous and had high yields. Figure out If It Is Elusive. Chelating and coordination were achieved using chemical tests and various spectral methods. The current measurements prove that the synthesized complexes portray the features of nonelectrolyte components, not the electrolyte substances. The stoichiometry of 1:1 directs either ligand to form a complex with the metal or not, as the characterization is elucidated by elemental and ESI-MS spectroscopic evaluation. The spectrum study revealed that the Cu (II) center is four-fold in the structure of the coordination complex. In addition, LANL2DZ basis sets, B3LYP correlation function, and DFT determine ligand involvement and molecular geometry of their complexes and resolve different inquiries positively. This research aimed to find out the electron stability level and the low gap in HOMO-LUMO energy, and finally, the chemical hardness of ligand complexes through the dipole moment, which are the contributing factors to the efficiency. Only the C0mplexes of Cr (III), Cd (II), Cu (II), and C0(II) exhibit non-planar symmetry, except for the plane-based CU(II). DFT predicted electrostatic potential for the atomic charge distribution in molecular compounds. Then, the model's computation was compared to the actual data source. The efficacy of the metal complex was investigated in these bacteria and fungal samples. Certain bacteria, which include *Staphylococcus aureus* and *Bacillus subtilis*, do not have cell walls that have the characteristic Gram-positive staining, while others, such as *Pseudomonas aeruginosa*, *Escherichia coli*, exhibit the Gram-negative reaction. The fungus *Aspergillus flavus* and *Candida*, in addition, may be present. The provided data indicates that the antibacterial compound exhibits favorable qualities. The most efficient artillery (II) system underwent a taste test involving various species. In addition, the anticancer capabilities of OTC2 and OTC4 complexes against MCF-7 (breast carcinoma) cells have been investigated. The investigation revealed that the [Cd (L) Cl₂ (H₂O)₂] complex demonstrated higher efficacy, with an IC₅₀ value of 36.14 μg/ml, surpassing the effectiveness of cisplatin. Compared to normal VERO cells and cisplatin, its exceptional selectivity for cancer cells was shown. This study aims to determine the strength of the interaction between different peptides and specific protein structures related to *Helicobacter pylori* glutamate racemase, MCF cells, and the COVID-19 viral protein. As a result, we performed molecular docking using three separate protein structures, namely 2JFZ, 3QX3, and 6XBH, each having distinct functionalities. The purpose of this study is to utilize molecular docking techniques to discover the precise binding pattern and different energies of ligands and metal C0mplex about MCF cell molecules and the COVID-19 viral protein receptor. The molecular docking investigation identifies weaknesses in the structural characteristics, which can be utilized to determine the binding mechanisms. These comprehensive evaluations highlight the various applications and fascinating biological attributes of the identified compounds, making them well-suited for further investigation into their inhibitory effects.

Keywords Anti: Schiff base complexes; Triazole; spectral studies; spectra Molecular docking; DFT; Antimicrobial activity; Anti-COVID-19; -H. pylori

1. Introduction

Schiff bases, which fall under the category of ligands, are a well-studied group of molecules that can bond with almost all elements in the periodic table [1]. Schiff base ligands are compatible with transition and non-transition metal ions, forming solid bonds by nitrogen and oxygenophilic attachment, making them ideal for chelation. One example of unique structurally produced ligands is Schiff bases (SBs) and their related metal (II) C0mplexes. These complexes contain azomethine (-CH=N-) links, which have a wide range of bioactive properties. This set of actions encompasses a range of notable physiological

*Corresponding author e-mail: shaimaa.mostafa.elgazar@gmail.com.; (Shaimaa M. Elgazar).

Received date 01 May 2024; Revised date 29 July 2024; Accepted date 30 July 2024

DOI: 10.21608/EJCHEM.2024.286517.9667

©2025 National Information and Documentation Center (NIDOC)

processes, such as [2], antifungal antibacterial [3], anticancer, anti-diabetic anti-inflammatory [4], [5], and antitumor impacts. Schiff bases exhibit significant anticancer action, which is attributed to the reactivity of the imine group [6]. The presence of nitrogen and oxygen molecules in substantial amounts may disrupt the DNA nitrogenous bases and cellular structures through the involvement of Schiff bases. This disruption can lead to mutations and be used as therapeutic resources for cancer management [7]. Moreover, Schiff base gel complexes are significant because they are easy to synthesize, have a variety of chemical structures, and are extensively used in fields such as material chemistry, molecular magnetics, catalysis, and biodynamic modeling [8]. Additionally, ligands of Schiff's base likely get their effectiveness from the presence of oxygen and nitrogen atoms and their side chains containing polar groups that facilitate interactions with several molecules in the body. The distinct behavior of metal Complex (MLs) may arise from the existence of unambiguously defined metal (M) ions and anions that lack dimensional properties. These components synergistically contribute to the increased adaptability of the complexes in their approach and interaction. Ligands that possess a minimum of two donor heteroatoms have gained recognition within scientific groups worldwide due to their intricate structure. They can create complexes with atomic states that are simple, di-, or multinuclear [9]. In metal-ligand reactions, the interaction between the lone pair of electrons of heteroatoms determines the bonding strength. The principal objective of the study is synthesis (E)-2-(2-(1-(1H-benz[d][1,2,3] triazole-1-yl)propan-2-ylidene)hydrazine)-2-iodoacetamide, a new SB ligand. During the synthesis step, the condensation reaction of these 1,1 diols with the aldehyde functions takes place. Experts are dedicated to employing cutting-edge techniques in physical/chemical analysis of the ligands formed in SB process together with many metals such as Cr (III), Cu (II), Co(II), and Cd (II). The author has taken a deep approach into the metabolic studies of SB ligand itself and its M.complexes to unearth their antibacterial, antifungal and anticancer effects. A molecular virtual screening strategy, mainly based on a docking approach, was applied to check the possibility of interaction between a ligand with Cd (II) compounds at 2JFZ, 3QX3, and 6XBH sites to obtain the molecular information for this interaction. The assignment was carried out using MOE software, a well-known method that has proven to be accurate and consistent in giving results.

2. Materials and Methods

2.1. Experimental

2.1.1. Chemicals and components

Through the use of carefully selected and refined chemicals, including 1-(1H-benz[d][1,2,3] triazole-1-yl) propane-2-one from Merck and hydrazone of diacetamidic acid from Sigma-Aldrich, we were able to work on the development of this diagnostic tool. In the mix, BDH organic solvents, cobalt (III) chloride dodecahydrate, copper (II) chloride, and often used in spectroscopy ethanol of spectroscopic grade, were also obtained. Pure water, which had been put into enclosed glass bottles, was strongly recommended for every test. A breast cancer cell line, MCF-7, preserved in a cryopreservation process using -180°C, was shipped from the American Type Culture Collection. Sub-population of the MCF-7 tumor cell line, originally from the Institute of Cancer in Cairo, Egypt, was cultured and maintained using the serial target-population technique.

2.1.2. Solutions

A solution with the concentration of 1×10^{-3} M of SB ligand (L) and the (ML) complexes mentioned recently has been prepared by accurately measured volumes of each in DMF (for Cu(II)) and ethanol (for the SB ligand (L)). The electrical conductivity of the metal Complex solution increases linearly with its concentration, which is 1×10^{-3} M. At the same time, the accurate concentrations of the SB ligand (Keim I) or its metal Complexes were prepared by precisely diluting the stock solution using meticulous method for the UV-Vis spectra analysis.

2.1.3. Solution of anticancer study

2.1.3.1. Viability assay "MTT protocol"

The MTT method [10-12] is employed for carrying out an in vivo viability experiment, which aims to assess the toxicity of chemicals on cultured cells. A 96-well plate was prepared for tissue culture with a 1 ml cell solution containing 1×10^5 cells/ml. The plate was then positioned in an incubator set at 38°C for 24 hours. This was done to promote the ongoing adherence of cells and the development of a fully formed layer of cells covering the whole surface of the plate.

The stage at which the sheets of cells are fully merged is followed by removing the growing media through aspiration. Afterward, the cell monolayer is washed twice using the wash media. Subsequently, the serum content was reduced to 2% from the standard 10%, and the RPMI maintenance medium was employed. The 0.1 ml diluted sample was added to specific wells, while the remaining three wells contained only the maintenance medium. After that, the plate was positioned in the incubator at a temperature of 38°C. The cellular morphology was then examined to determine toxic effects, which might indicate the partial or total loss of the monolayer, cell rounding, shrinkage, or granulation. To create a diluted MTT solution with a concentration of 5 mg/ml in PBS, 20 μ L of the solution was added to each well. To ensure proper mixing of MTT into the fluid, the plate was shaken on the table at 150 rpm for 5 minutes. Subsequently, a 5-hour incubation at 38°C with 5% CO₂ was performed to allow metabolic-capable cells to transform the MTT reagent into purple-colored formazan crystals. Next, the MTT (metabolic product of MTT) was extracted from the well and suspended in 200 μ L of DMSO. The suspension was then subjected to shaking on a table at a speed of 150 rpm for an additional 5 minutes. Finally, optical density measurements

were acquired at a wavelength of 560nm, with the result at 620nm as the reference. This investigation demonstrated the correlation between the optical density, measured straight from the cells, and the number of live cells.

2.1.4. Instrumentation

The quantitative examination of the primary elemental composition (carbon, hydrogen, and nitrogen) was performed at a Microanalytical Center in Egypt affiliated with the Faculty of Science at Cairo University. The primary instrument used for analysis was the CHNS-932 (LECO) Vario. The XMTD-3000 equipment was used to determine the melting point. The Egyptian Petroleum Industry Research Institute employed the inductively coupled plasma atomic absorption spectrometry (ICP) method to determine trace metals' content. The Perkin-Elmer 1650 FT-IR spectrometer, operating in the 4000 to 400 cm^{-1} spectral range, conducted infrared (IR) spectroscopic investigations using KBr pellets. The conductivities of DMF solutions containing solid complexes with a concentration of 10⁻³ M were measured using a Jenway 4010 conductivity meter. Hydrogen nuclear magnetic resonance (NMR) experiments using DMSO-d₆ were conducted on a 300MHz Varian-Oxford Mercury spectrometer. An internal standard, tetramethylsilane, was used, and the experimental temperature was set to room temperature. The user employed the electron ionization technique at 70 eV using an MS-5988 gs-ms Hewlett-Packard instrument to generate mass spectra. This instrument is accessible for usage at the Microanalytical Center at Cairo University. The Schiff base ligand and the metal complex thermal analysis were performed using the Shimadzu TG-50H equipment. This analysis included TG-TAC and TGM measurements; thermal-loaded diagrams represented the results. The measurements were conducted across a temperature range from ambient to 1,000 °C. The spectrophotometers were investigated using a solution-based approach. The PerkinElmer Model Lambda 20, an automatic UV-Vis spectrophotometer, was used. It covered a wavelength range of 200 nm to 700 nm. Experiments were conducted at the National Cancer Institute to evaluate the cancer-fighting potential of M.HR. The Cancer Biology and Pharmacology Departments of Cairo University in Egypt conducted the experiments. The antimicrobial properties were assessed at Cairo University's Microanalytical Center, our primary facility for evaluating microbial activity.

2.2.Synthesis of SB Ligand and Its (ML) Complexes: Methodology and Preparation

The novel SB ligand, referred to as (SBL), underwent elemental analyses, as detailed in Table 1, encompassing nitrogen (N), hydrogen (H), and carbon (C) alongside corresponding melting points. The results data are reliable, with the actual values derived from the proposed molecular formula affirming the accuracy of the synthesis process. The distinct melting points observed further confirm the purity of the synthesized SB L and its (ML) complexes. The synthetic pathway for the Schiff base is elucidated in Scheme 1. Structural confirmation of the SB ligand is established through comprehensive analyses of infrared (IR) and proton nuclear magnetic resonance (¹H NMR) spectra, with an in-depth discussion reserved for the associated metal complex [13]. The Schiff base ligand exhibits a unique yellowish-brown color, demonstrating stability at ambient temperature and solubility in dimethyl sulfoxide (DMSO) and DMF solvents. The agreement between the experimental results and the proposed formula underscores the reliability of the obtained data. Scheme 1 provides a visual representation of the structural configuration of the SB ligand. Assessment of the metal-to-ligand ratio in all complexes, based on carbon, hydrogen, nitrogen, and metal content, suggests a 1:1 ratio (Table 1), following an M: L configuration. Experimental elemental analyses for the complexes closely match theoretical calculations (Table 1), validating the proposed formula [14]. Characterization of the metal complex of the bidentate SB ligand involves diverse analytical techniques, including elemental analyses, molar conductivity, infrared spectroscopy (IR), proton nuclear magnetic resonance (¹H NMR), ultraviolet-visible spectroscopy (UV–Vis), mass spectrometry, and thermal analyses. The suggested structures are visually depicted in Figure 1.

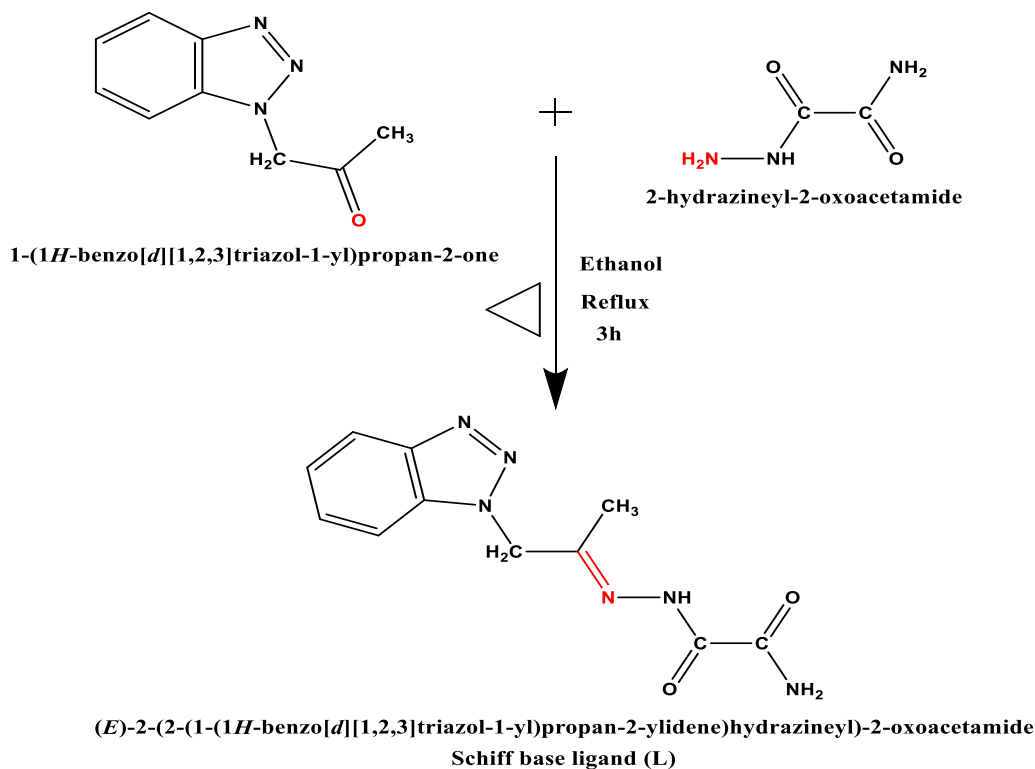
2.2.1. Preparation of SB ligand

The efficient synthesis of the new Schiff base ligands, designated as (L), was carried out using the described pathway [14]. Outlining the approach for this task required condensing the reaction of 1-(1H-benzo[d][1,2,3]triazole-1-yl) propane-2-one (2.85 mmol, 0.5 g) and 2-hydrazineyl-2-oxoacetamide (2.85 mmol, 0.5 g). The reaction mixture underwent a wide range of transit for 4 hours. After removing ethanol, filtering, and recrystallizing the yellow solid, the final product obtained was a pure Schiff base, yielding 87%.

The diagram depicted the arrangement of the SB ligand and the reactive side involved in its production process. The resulting product was a brownish, solid crystalline material with a melting point of 207°C and an 87% yield. The elemental analysis yielded the following results for C₁₁H₁₂N₆O₂ (%): The composition of the substance is as follows: Carbon (C) accounts for 50.77%, Hydrogen (H) accounts for 4.65%, Nitrogen (N) accounts for 32.29%, and Oxygen (O) accounts for 12.29%. The experimental study resulted in the following percentages: Carbon (C) - 50.49%, Hydrogen (H) - 4.37%, Nitrogen (N) - 32.01%.

Through the application of forensic infrared spectroscopy (IR), we were able to identify distinct peaks at specific wavenumbers: 3383 cm^{-1} (representing NH₂ stretching), 3173 cm^{-1} (representing NH stretching), 1635 cm^{-1} (representing C=N stretching), and 1675 cm^{-1} (representing $\nu(\text{C}=\text{O})$ vibration).

The drop characteristic was verified using UV–visible spectroscopy, which detected absorption bands at 295 nm, 329 nm, and 398 nm. These wavelengths correspond to the π – π^* transition, n – π^* transition, and charge transfer.



Scheme 1. Synthesis Pathway of SB ligand

2.2.2 Synthesis of Binary Schiff Base Complexes

The synthesis method for Cr (III), Co(II), Cu(II), and Cd(II) complexes involved the reaction of equal molar amounts of metal chloride (1.53 mmol) with the SB ligand (0.4 g, 1.53 mmol) in a heated ethanolic solution at 60 °C. The mixture was subjected to reflux for 4 hours, forming the complexes through precipitation. Filtration was employed for gathering, followed by purification by successive diethyl ether rinses. Scheme (2) depicts the structural arrangement of the metal C0mplex formed by the binary SB ligand and demonstrates the process involved in their creation.

2.2.2.1. [(L) Cr Cl₃ (H₂O)]

A dark blue crystalline solid with a melting point of 243°C was produced with an 87% yield. The molecular formula, (C₁₁H₂₀Cl₂CoN₆O₆), was determined using elemental analysis, with calculated and observed percentages as follows: The percentages of C, H, Cr, Cl, and N are as follows: C (28.29% vs. 28.03%), H (4.36% vs. 4.09%), Cr (12.75% vs. 12.34%), Cl (15.34% vs. 15.12%), and N (18.18% vs. 17.78%). The compound displayed a molar conductivity (Λ_m) value of 39 $\Omega^{-1} \text{ mol}^{-1} \text{ cm}^2$. The infrared spectroscopy analysis (FT-IR) showed distinct peaks at certain wavenumbers: 3384 cm^{-1} (corresponding to NH₂ stretching), 3173 cm^{-1} (representing NH stretching), 1611 cm^{-1} (indicating Azomethine C=N), 1669 cm^{-1} (associated with C=O), 527 cm^{-1} (representing metal-oxygen, M-O), 426 cm^{-1} (indicating metal-nitrogen, M-N), and 332 cm^{-1} (corresponding to metal-chlorine, M-Cl). The UV-Vis spectroscopy results revealed absorption bands at 257 nm corresponding to $\pi-\pi^*$ transitions, 312 nm corresponding to $\pi-\pi^*$ conjugated transitions, 336 nm according to $n-\pi^*$ transitions, and 392 nm corresponding to charge transfer.

2.2.2.2. [(L) Co Cl₂ (H₂O)₂].2H₂O

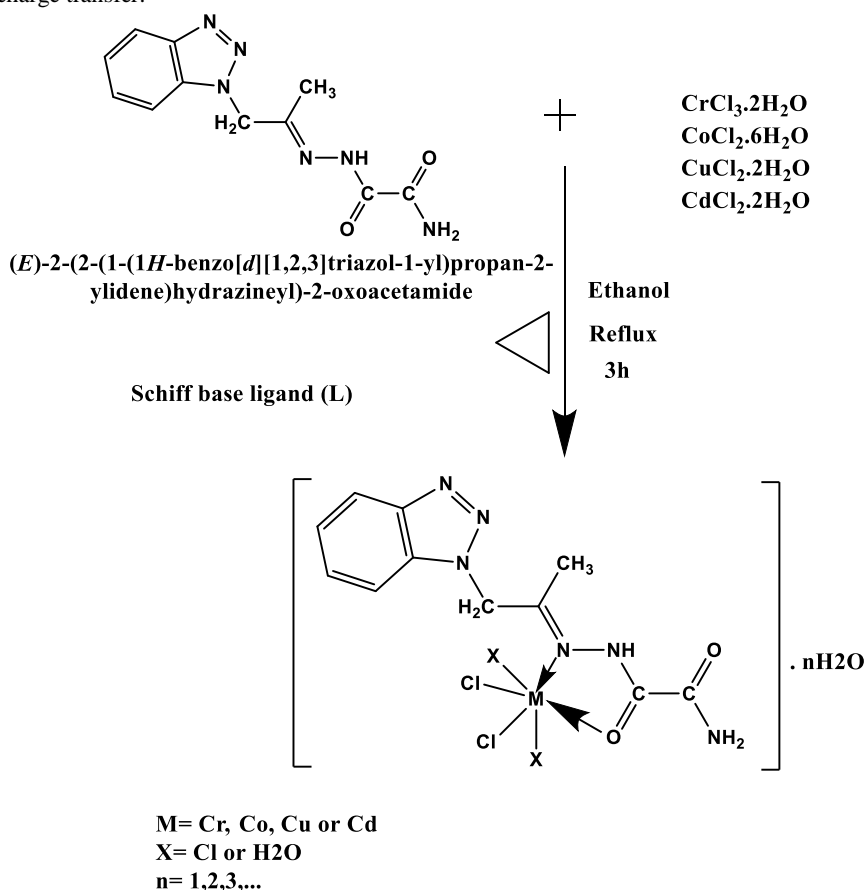
A dark brown crystalline solid with a melting point of 229°C was produced with an 81% yield. The molecular formula, (C₁₁H₁₄Cl₃CrN₆O₃), was determined using elemental analysis, with calculated and observed percentages as follows: The existence of C, H, Co, Cl, and N are 30.26%, 3.23%, 11.91%, 24.36%, and 19.25% respectively, compared to 29.87%, 3.04%, 11.63%, 24.17%, and 19.09%. The compound displayed a molar conductivity (Λ_m) of 26 $\Omega^{-1} \text{ mol}^{-1} \text{ cm}^2$. The FT-IR analysis showed distinct peaks at certain wavenumbers: 3382 cm^{-1} for NH₂ stretching, 3173 cm^{-1} for NH stretching, 1609 cm^{-1} for Azomethine C=N, 1667 cm^{-1} for C=O, 535 cm^{-1} for metal-oxygen (M-O), 424 cm^{-1} for metal-nitrogen (M-N), and 357 cm^{-1} for metal-chlorine (M-Cl). UV-Vis spectroscopy revealed absorption peaks at 240 nm according to $\pi-\pi^*$ transitions, at 305 nm corresponding to $\pi-\pi^*$ conjugated transitions, at 339 nm corresponding to $n-\pi^*$ transitions, and 412 nm corresponding to charge transfer.

2.2.2.3. [(L) Cu Cl₂].2H₂O

A crimson crystalline substance with a melting point of 210°C was produced with a yield of 79%. The chemical formula, (C₁₁H₁₆Cl₂CuN₆O₄), was determined using elemental analysis, with calculated and observed percentages as follows: The existence of C, H, Cu, Cl, and N are as follows: C (30.67% vs. 30.35%), H (3.74% vs. 3.39%), Cu (14.75% vs. 14.29%), Cl (16.46% vs. 16.28%), and N (19.51% vs. 19.18%). The compound displayed a molar conductivity (Λ_m) of 17 $\Omega^{-1} \text{ mol}^{-1} \text{ cm}^2$. The infrared spectroscopy analysis (FT-IR) detected distinct peaks at certain wavenumbers: 3387 cm^{-1} (corresponding to NH₂ stretching), 3180 cm^{-1} (NH stretching), 1618 cm^{-1} (Azomethine C=N), 1670 cm^{-1} (C=O), 559 cm^{-1} (representing metal-oxygen, M–O), 422 cm^{-1} (indicating metal-nitrogen, M–N), and 361 cm^{-1} (signifying metal-chlorine, M–Cl). The UV-Vis spectroscopy results showed absorption bands at 247 nm corresponding to $\pi-\pi^*$ transitions, 303 nm corresponding to $\pi-\pi^*$ conjugated transitions, 343 nm according to $n-\pi^*$ transitions, and 419 nm corresponding to charge transfer.

2.2.2.4. [(L) Cd Cl₂ (H₂O)₂]

A brownish-yellow crystalline solid with a melting point of 198°C was produced with an 88% yield. The chemical formula, (C₁₁H₁₆Cl₂CdN₆O₄), was determined using elemental analysis, with calculated and observed percentages as follows: The existence of C, H, Cd, Cl, and N are 27.55%, 3.36%, 23.44%, 14.78%, and 17.52%, respectively, compared to the previous values of 27.23%, 3.12%, 23.19%, 14.28%, and 17.18%. The chemical demonstrated a molar conductivity (Λ_m) of 33 $\Omega^{-1} \text{ mol}^{-1} \text{ cm}^2$. The results of infrared spectroscopy (FT-IR) showed distinct peaks at certain wavenumbers: 3381 cm^{-1} (corresponding to NH₂ stretching), 3171 cm^{-1} (representing NH stretching), 1623 cm^{-1} (indicating Azomethine C=N), 1669 cm^{-1} (denoting C=O), 534 cm^{-1} (representing metal-oxygen, M–O), 426 cm^{-1} (indicating metal-nitrogen, M–N), and 345 cm^{-1} (representing metal-chlorine, M–Cl). The UV-Vis spectroscopy revealed absorption bands at 236 nm according to $\pi-\pi^*$ transitions, at 317 nm equivalent to $\pi-\pi^*$ conjugated transitions, at 351 nm equivalent to $n-\pi^*$ transitions, and at 422 nm corresponding to charge transfer.



Scheme 2. Schiff base metal complex formation

2.2.3. Exploration of Spectrophotometric Analyses

Absorption spectra were recorded for solutions containing the uncomplexed SB ligand and its metal coordination complexes, each maintained at a $1 \times 10^{-4} \text{ M}$ concentration. The spectral analysis encompassed the wavelength range of 200 to 700 nm.

2.2.4. Methodical Computational Approach

The molecular geometry of an SB ligand and its matching Cd (II) complex was optimized, and the structural energy was determined using density functional theory (DFT) with the GAUSSIAN09 program, Version 9.5, and GAUSSVIEW 6.0.16 [15,16]. The computational method used was the B3LYP hybrid exchange-correlation functional and the Lan12dz basis set. The DFT/B3LYP approach is widely recognized for its efficacy in precisely computing electronic characteristics in organic systems, especially those that include electronegative atoms [17, 18]. The E (HOMO) and E (LUMO) energies, along with the ΔE , were computed to yield crucial insights into the ligand's electronic structure and reactivity.

2.2.5. Pharmacology

2.2.5.1. Antimicrobial activity

The antibacterial efficacy of the compounds was assessed using the agar well diffusion method [19]. The in vitro assessments of antibacterial properties involved testing against specific Gram-positive bacterial strains, namely *Staphylococcus aureus* (ATCC: 13565) and *Bacillus subtilis* (ATCC: 6633), as well as Gram-negative bacteria, including *Escherichia coli* (ATCC: 10536) and *Pseudomonas aeruginosa* (ATCC: 15442). The assessments were conducted utilizing a nutritious agar medium. The antifungal activity was assessed using a methodology outlined in prior studies [20]. The fungal strains *Candida albicans* (ATCC: 10231) and *Aspergillus niger* (ATCC: 16404) were analyzed using the Sabouraud dextrose agar medium. The comparison study utilized standard medications: Ampicillin for Gram-positive bacteria, Gentamicin for Gram-negative bacteria, and Nystatin for fungal strains—the negative control employed dimethyl sulfoxide (DMSO) as the solvent. The compounds were assessed at a 15 mg/ml concentration against bacterial and fungal strains. Instead, agar-based methods, such as E-testing and disc diffusion, were chosen due to their faster and more direct evaluations than broth-based procedures [21].

2.2.5.2. Method of testing

Aseptic culture media, roughly 20-25 mL per Petri plate, were poured and left to harden at room temperature. A suspension of microorganisms, corresponding to the McFarland 0.5 standard solution (1.5×10^5 CFU mL⁻¹), was produced in sterile saline. The turbidity of the suspension was adjusted to an optical density (OD) of 0.13 at 625 nm using a spectrophotometer [22]. Afterward, within a 15-minute of adjusting the cloudiness, a clean cotton swab was dipped into the produced mixture and evenly spread on the dried agar surface. The swab was allowed to dry in the air for 15 minutes while the lid was firmly closed. By employing a sterile borer, wells with a diameter of 6 mm were created in the solidified material [22]. Subsequently, a precise volume of 100 μ L of the test compound solution was added to each well using a micropipette. The Petri plates were incubated at 37°C for 24 hours to assess their antibacterial effectiveness. The experimental methodology was replicated thrice, and the inhibition zones were quantified in millimeters [22].

2.2.5.3. Antitumor efficacy

The cytotoxicity of the SB ligand and its (ML) complexes was evaluated using the Skehan and Storeng technique [23]. Before the experiment, the compounds were diluted at different concentrations (31.25, 62.5, 125, 250, 500, and 1000 μ g/ml) and incubated for 24 hours on a 96-well plate. This allowed the compounds to adhere to the cells. After incubation, a layer of cells and the chemicals were cultivated for 48 hours at 37°C with a CO₂ concentration of 5%. After incubation, the cells were fixed, washed, and stained with SRB. The excess stain was eliminated using Tris-EDTA buffer and acetic acid, followed by the recovery of the stain. All samples' optical density (OD) was measured at 564 nm using an ELISA microplate reader. Automated background corrections were implemented, and average values were calculated for each medication concentration. The relationship between the concentration of drugs and the fraction of cells that survived was established, resulting in survival curves for each substance in the breast carcinoma cell line. The control group comprised untreated MCF7 breast cancer cell lines, whereas the positive control group consisted of MCF7 breast cancer cell lines that were treated with the conventional medication Cisplatin. After completing the experiment, the survival curves offered valuable insights into the effects of various drugs on breast carcinoma cell lines [10-12]. To evaluate the impact of the compounds on the survival of cells, a relationship was created between the fraction of cells that survived and the concentration of the given drug. The execution of this procedure led to the creation of a survival curve tailored to the particular breast carcinoma cell line being studied. The cell survival percentage was calculated using the following formula:

$$\text{Survival fraction} = \frac{\text{O.D. of treated cells}}{\text{O.D. of control cells}}$$

The main aim of this work was to establish the IC₅₀ values, which indicate the concentrations of the Schiff base ligand or its metal complex required to suppress cell growth by 50%. The complete experimental technique was replicated thrice rigorously, specifically for the MCF7 cell line, to improve the reliability and consistency of the acquired results.

2.2.6. Molecular docking

The MOE 2014 software, renowned for its proficiency in inflexible molecular docking, was employed to conduct molecular docking research. The analyses significantly predicted the likely ways the SB ligand and its chosen binary Cd (II) complex bind, as they had increased biological activity against essential receptors. The work focused on analyzing the crystal

structures of significant receptors, including the crystal structure of *Helicobacter pylori* glutamate racemase in conjunction with D-Glutamate and an inhibitor (PDB ID: 2JFZ). The number 24 is enclosed in square brackets. The crystal structure of Human topoisomerase IIbeta complexed with DNA and etoposide (PDB ID: 3QX3) plays a vital role in cancer therapy. The Main Protease (Mpro) of SARS-CoV-2 is another essential structure that is a crucial target for antiviral medicines. The crystal structure of the SARS-CoV-2 (COVID-19) primary protease bound to the inhibitor UAW247 (PDB ID: 6XBH) illustrates this. The number 26 is enclosed in square brackets. The software requires input in PDB format, which consists of the SB ligand, the binary Cd (II) complex, and the receptors. During the preparation of the input files, extraneous elements such as water molecules, co-crystallized ligands, and unsupported components like Na, K, Hg, etc., were eliminated. However, the amino acid chains were conserved for subsequent analysis [27]. The Schiff base ligand and its specific binary Cd (II) complex were generated in PDB file format using the Gaussian tool. The crystal structures of all receptors were acquired from the Protein Data Bank (PDB), accessible at <http://www.rcsb.org/pdb>. This methodology elucidates the precise location of the ligand and receptor binding sites and the specific nature of the interactions between them. Additionally, it provides an approximate assessment of the distance between the ligand and the receptor within the interaction grid. The scoring energy at each position, as determined by the docking computations, reflects the degree of inhibition induced by the corresponding ligand. This work offers significant insights into potential medical uses. In summary, our study employed a well-established method to assess the harmful impacts of the Schiff base ligand and its Cd (II) metal complex. The study utilized several concentrations and analytical techniques to evaluate their influence on the growth of breast cancer cells. The IC50 values were used to assess these substances' efficacy in inhibiting cell growth. The experiment was carefully replicated to enhance the scientific validity of the results.

2. FINDINGS AND ANALYSIS

The SB ligand and their corresponding binary (ML) complexes were extensively characterized using various techniques. These included elemental analysis, molar conductance measurement, UV-visible spectroscopy, Fourier-Transform Infrared (FT-IR) spectroscopy, Mass spectrometry, ¹H Nuclear Magnetic Resonance (NMR) spectroscopic analysis, and Thermal analysis studies, specifically Thermogravimetric Analysis (TG) and Derivative Thermogravimetry (DTG). The results of these assessments are briefly described progressively.

3.1. Characterization of an SB ligand

The elemental analysis results indicate that the newly synthesized ligand, referred to as the SB ligand, closely corresponds to the calculated values for carbon (C), hydrogen (H), and nitrogen (N). The chemical formula of the ligand is C₁₁H₁₂N₆O₂, which aligns with the suggested formula. At room temperature, the SB ligand is stable and can be dissolved in DMSO and DMF. The mass spectrum of the SB ligand confirms its proposed formula by showing a peak at 260.26 amu for the molecular ion (m/z). This peak confirms that the ligand comprises C₁₁H₁₂N₆O₂, with an atomic mass of 261.11 amu. Multiple peaks belonging to separate fragments of the SB ligand are also recorded. The ¹H NMR spectra of compound L display several signals for the protons in the aromatic ring, which are observed in the range of 7.3-8.076 ppm [28]. In addition, a signal at 10.703 ppm, which is associated with the –NH proton signal, is observed as a singlet (1H) [29] (see Table 3). The lack of evidence for the NH₂ group in the free amine molecule, coupled with the detection of a signal at 7.66 ppm for the NH₂ group directly bonded to the carbonyl group (C=O), confirms the synthesis of the Schiff base ligand. The existence of the azomethine group and the successful production of the Schiff base product are confirmed by the characteristic band observed at 1625 cm⁻¹ in the Schiff base ligand's infrared (IR) spectra [30]. The observation is supported by Density Functional Theory (DFT) analysis, which accurately captures the peak at 1660 cm⁻¹. The strong correlation between the frequencies observed in experiments and those calculated The successful synthesis of the Schiff base ligand is theoretically confirmed, as depicted in Figure 1. The observed differences between the theoretical and experimental frequencies may be attributed to systematic errors, which could be associated with factors such as harmonicity or the incorporation of gas-phase molecules in DFT calculations. To minimize the chances of these potential errors, a correlation coefficient of 0.9648 was employed for LAN2DZ [31, 32] to enhance the accuracy and reliability of the obtained results.

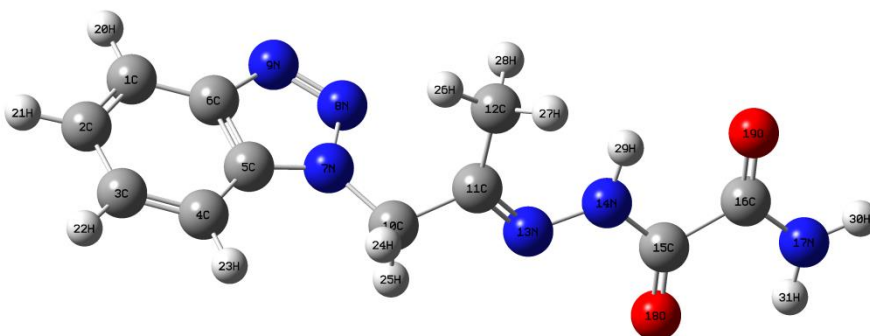


Fig.1. The optimized geometry configuration of the SB ligand

3.2. Analysis of Binary Metal Complex Formed with Schiff Base: Characterizing Their Properties

3.2.1. Elemental analysis

The mixture of metal salts with an SB ligand led to the creation of binary metal Complex, obtained with high efficiency in a 1:1 ratio (metal to ligand). The metal Complex exhibited solubility in various organic solvents, such as methanol, dimethylformamide (DMF), and dimethyl sulfoxide (DMSO). Table 1 contains a thorough analysis of the findings and presents the data in a clear and detailed manner. Therefore, this result creates an intricate structure with M: L ratio.

Table 1 Comprehensive Analysis of Analytical and Physicochemical Properties of an SB ligand and Its Corresponding Metal Complex.

Compound (chemical formula)	Color Yield (%)	M.p. (°C)	Found (Calc.)					Λ_m ($\Omega^{-1} \text{ mol}^{-1} \text{ cm}^2$)
			C (%)	H (%)	N (%)	Cl (%)	M (%)	
SB ligand	yellowish	138	50.48	4.37	31.98			
	brown 87%		(50.77)	(4.65)	(32.29)
[(L) Cr Cl3 (H2O)]	dark blue	243	28.03	4.09	17.78	15.12	12.34	
	87%		(28.29)	(4.36)	(18.18)	(15.34)	(12.75)	39
[(L) Co Cl2 (H2O)2].2H2O	dark brown	229	29.87	3.04	19.09	24.17	11.36	
	81%		(30.26)	(3.23)	(19.25)	(24.36)	(11.91)	26
[(L) Cu Cl2].2H2O	dark red	210	30.35	3.39	19.18	16.28	14.29	
	79%		(30.67)	(3.74)	(19.51)	(16.46)	(14.75)	17
[(L) Cd Cl2 (H2O)2]	Brownish-	198	27.23	3.12	17.18	14.28	23.19	
	yellow 88%		(27.55)	(3.36)	(17.52)	(14.78)	(23.44)	33

3.2.2. Molar conductivity measurements

The correlation equation $\Lambda_m = K/C$ can be used to calculate binary complexes' molar conductance (Λ_m). Here, C represents the molar concentration of solutions containing metal Complex. The SB ligand acts as a bidentate ligand with a neutral nature. The chelates were dissolved in dimethyl sulfoxide (DMSO), and the molar conductivities of solutions with a concentration of 10^{-3} M were determined at 25 ± 1 °C using established methods. The molar conductance values for chelates of Cr (III), Co (II), Cu (II), and Cd (II) range from 17 to $39 \Omega^{-1} \text{ mol}^{-1} \text{ cm}^2$, as shown in Table 1. The data suggest that these metal Complex have a non-electrolytic characteristic, consistent with previous studies [34, 35].

3.2.3. FT-IR spectral studies

The infrared (IR) spectra of the studied (ML)complexes were systematically compared to those of the unbound ligand to assess the coordination site's involvement in chelation. This evaluation is detailed in Table 2. The SB ligand displayed a prominent peak at 1625 cm^{-1} in its infrared spectra, indicating the presence of the azomethine $\nu(\text{C}=\text{N})$ group [36]. The band in question experienced a notable shift in frequencies within the range of $1609\text{--}1623 \text{ cm}^{-1}$ in the spectra of all complexes. This indicates that the azomethine nitrogen formed coordination bonds with the metal ions. The complexes exhibited broad bands from 3381 to 3387 cm^{-1} and 3171 to 3180 cm^{-1} , corresponding to the stretching vibration of the $\nu(\text{NH}_2)$ and $\nu(\text{NH})$ groups, respectively. This observation suggests the presence of synchronized water molecules across a broad range [37]. The infrared spectra of the SB ligand showed a peak at 1675 cm^{-1} , which was attributed to the $\nu(\text{C}=\text{O})$ functional group. After the complex was formed, there was a shift in the frequency of this band to a range of $1667\text{--}1670 \text{ cm}^{-1}$ [36], indicating that the oxygen of the $(\text{C}=\text{O})$ group bonded with the metal ions [38]. The complexes displayed supplementary bands within the $527\text{--}559 \text{ cm}^{-1}$ spectral range, originating from the vibrational mode $\nu(\text{M}-\text{O})$. Additional bands were observed in the $424\text{--}426 \text{ cm}^{-1}$ range, which can be attributed to the vibrational mode $\nu(\text{M}-\text{N})$ [38-42]. Furthermore, bands were observed in the $332\text{--}361 \text{ cm}^{-1}$ region, emanating from the vibrational mode $\nu(\text{M}-\text{Cl})$.

The SB ligand demonstrated monovalent bidentate chelation by serving as a chelating agent. It bonded to the metal ion by utilizing one oxygen atom from the carbonyl $(\text{C}=\text{O})$ group and one nitrogen atom from the azomethine group of the Schiff base. The configuration of three or two water molecules and a chlorine atom in all complexes resulted in octahedral complexes, except the Cu complex, which exhibited a square planar geometry.

Table 2. The most significant infrared (IR) spectral bands of the isolated SB ligand binary Complexes are as follows:

Compound	ν [NH ₂]	ν [NH]	ν [C=N]	ν [C=O]	ν [M-N]	ν [M-O]	ν [M-Cl]
SB ligand	385 br	3173 br	1625 m	1675 sh	
(1) [(L) Cr Cl ₃ (H ₂ O)]	3384 br	3173 br	1611 m	1669 sh	426w	527 w	332
(2) [(L) Co Cl ₂ (H ₂ O) ₂].2H ₂ O	3382 br	3173 br	1609 w	1667 sh	424 w	535 w	357
(3) [(L) Cu Cl ₂].2H ₂ O	3387 br	3180 br	1618 w	1670 sh	422 w	559 w	361
(4) [(L) Cd Cl ₂ (H ₂ O) ₂]	3381 br	3171 br	1623 sh	1669sh	426 w	534 w	345

Sh=sharp, br=broad, w=weak.

3.2.3. Mass spectral studies

The metal C0mplex produced with the Schiff base (referred to as L) was analyzed using mass spectrometry. The analysis revealed clear peaks corresponding to molecular ions, as described in Table 3. Examination of the mass spectral data confirmed the precise chemical composition of the metal complex, represented as [M (L) (H₂O)_n (Cl)_m]. xH₂O. In addition, the results acquired from these examinations perfectly agreed with the expected molecular formulas. This agreement was further supported by the data from elemental analysis, which can be found in Table 1.

Table 3: Exploration of Extensive Datasets About Schiff Base Ligands (L) and Their Respective Metal C0mplex.

Compound	m/z value		Interpretation
	Calculated	Found	
SB ligand	260.26	261.11	[M+1] ⁺
(1) [(L) Cr Cl ₃ (H ₂ O)]	436.62	436.90	[M+1] ⁺
(2) [(L) Co Cl ₂ (H ₂ O) ₂].2H ₂ O	462.15	463	[M+1] ⁺
(3) [(L) Cu Cl ₂].2H ₂ O	534.35	535.80	[M+1] ⁺
(4) [(L) Cd Cl ₂ (H ₂ O) ₂]	479.60	479	[M] ⁺

3.2.5 ¹H-NMR spectral studies

Examining ¹H-NMR spectra supports the suggested bonding configuration in the produced compounds. The ¹H-NMR spectra of the synthesized SB ligand and its Cd (II) complex were obtained in DMSO-d₆, and the associated chemical shift values (ppm) were determined. The ligand spectrum revealed multiple signals in the 7.3-8.076 ppm region attributed to the aromatic group.

Additionally, a signal at 5.784 ppm was allocated to the CH₂ proton, as indicated in Table 3. The signals were also observed in the Cd (II) complex, with chemical shifts of 7.36-8.06 ppm and 5.654 ppm, respectively. In addition, the proton signals of the NH group appeared as singlets at a chemical shift of 10.703 ppm in the Schiff base ligand (L1). The signals remained present in the Cd (II) complex but saw a displacement toward higher levels, measuring 10.81 ppm. In addition, the proton signals originating from NH₂ were detected as singular peaks at 7.913 ppm in the SB ligand. In the Cd (II) complex, the signals remained distinguishable but were displaced to a lower value at 7.66 ppm, indicating the occurrence of chelation. This information can be found in Table 3.

The protons originating from CH₃ were observed at a chemical shift of 2.493 ppm but were subsequently shifted to a lower value of 2.381 ppm. This discovery indicates that chelation took place in the Cd (II) complex by attaching it to the nitrogen atom of the C=N group.

Table 3 presents the ¹H NMR spectral data for the Triazole SB ligand and its binary Cd (II) metal complex.

Compound	Chemical shift, (δ) ppm	Assignment
Schiff base ligand (L)	10.703	(s, H, NH)
	7.913	(s, 2H, NH2)
	2.493	(s, 3H, CH3)
	5.784	(s, 2H, CH2)
	7.3-8.076	(m, 4H, aromatic)
[(L) Cd Cl ₂ (H ₂ O) ₂]	7.36-8.06	(m, 4H, aromatic)
	5.654	(s, 2H, CH ₂)
	10.81	(s, H, NH)
	2.381	(s, 3H, CH ₃)
	7.66	(s, 2H, NH ₂)

3.2.4. Spectroscopic Analysis of the UV–Visible Absorption Profiles for the SB Ligand and Its (ML) complexes.

An analysis showed the electronic spectra of an SB ligand that binds to two sites and its (ML) complexes in a range of 200 to 700 nm wavelengths in an appropriate solvent. When seen independently, the UV-Vis spectra of the SB ligand showed three separate absorption bands at 240, 328, and 381 nm. The observed absorptions were ascribed to distinct transitions: the absorption at 240 nm was related to $\pi-\pi^*$ transitions, the absorption at 328 nm represented $n-\pi^*$ transitions within the $-C=N-$ group, and the absorption at 381 nm was associated with charge transfer processes [43, 44]. The 240 nm band in the SB ligand spectra changed its position to higher or lower wavelengths within the range of 236-257 nm when it formed complexes with different metal cations. This indicates changes in the $\pi-\pi^*$ transitions for all the complexes. In addition, the band associated with the azomethine group first detected at 328 nm in the ligand spectrum, shifted to the range of 336-351 nm, indicating alterations in $n-\pi^*$ transitions [45]. The spectrum data indicates a substantial role of the nitrogen azomethine ($C=N-$) in coordinating with the metal ions. In addition, the band seen at 381 nm in the ligand shifted towards longer wavelengths in all binary complexes, with a range of 392 to 422 nm.

3.2.6. Thermal analysis of ternary SB ligand and its (ML) complexes.

The analysis utilized thermal geometric analysis (TGA) to assess the thermal stability of the produced metal complex and determine whether water molecules were present in their hydrated or coordinated molecular structures [46, 51]. Thermal and Derivative Thermogravimetric investigations were conducted on the metal complex produced with the SB ligand, investigating their response to varying temperatures from room temperature to 800°C. The findings included data on temperature ranges, decomposition stages, product loss throughout decomposition, comparison of calculated and observed weight loss percentages, and residues of all components, as detailed in Table 4. The TG thermogram analysis of the [(L) Cr Cl₃ (H₂O)] complex reveals a breakdown mechanism that occurs in two distinct phases. The first three phases occur within a temperature range of 20-245°C, with the highest point at 221.63°C. During these stages, H₂O, Cl₂, and C₂H₅NO molecules are released, leading to a weight loss of 33.506% (33.87%). The following stages, taking place at temperatures ranging from 245 to 800°C with maximum points at 352.33 and 450.45°C, entail the removal of the coupled C₉H₇Cl N₅ molecule, resulting in a weight reduction of 50.237% (calculated as 50.53%). The byproduct of breakdown is recognized as Chromium oxide ($\frac{1}{2}Cr_2O_3$). The thermal decomposition investigation of the [(L) Co Cl₂ (H₂O)₂].2H₂O complex reveals that the initial decomposition phase takes place between 35-160°C, with a peak at 98°C. The liberation of coordinated water molecules characterizes this phase. The determined mass reduction was 7.50%, which corresponds to the anticipated value of 7.78%. The second breakdown phase occurred within the temperature range of 160-485°C, with the highest point at 325°C. This phase involved the dissociation of C₉H₁₃Cl₂N₃O₂, leading to a loss of mass equal to 57.09% (calculated as 57.57%). The last stage of decomposition occurred between temperatures of 485-800°C, with the highest point at 595.21°C. During this stage, C₂H₃N₃O was eliminated, resulting in a mass loss of 18.22% (estimated as 18.40%). The remaining product after decomposition was cobalt oxide (CoO). In three stages, the [(L) Cu Cl₂].2H₂O complex underwent heat deterioration. The first phase, which occurred between temperatures of 30-150°C and reached its highest point at 96°C, led to a reduction in mass of 7.832% (estimated as 8.35%). The elimination of two water molecules caused this decrease in mass. The ensuing decomposition, which occurred at temperatures ranging from 150 to 410°C and exhibited several peaks, resulted in the release of C₉H₁₁N₄OCl₂, causing a mass loss of 60.223% (calculated as 60.84%). The last phase, occurring between temperatures of 410-800°C and peaking at 494.43°C, involved the release of C₂H₂N₂, leading to a loss of mass up to 12.414% (calculated as 12.76%). The remaining substance after decomposition consisted of copper oxide (CuO). The [(L) Cd Cl₂ (H₂O)₂] complex underwent early breakdown in the temperature range of 35-210°C, with distinct peaks observed at 120.17 and 198.69°C.

These peaks indicate the elimination of 2H₂O, resulting in an estimated mass loss of 7.03% (calculated as 7.50%). The second phase, occurring at temperatures ranging from 210–370°C with a peak at 247.266°C, involved the decomposition of C₆H₄N₃Cl, leading to a weight loss of 31.75% (calculated as 32.02%). The ultimate breakdown, occurring between temperatures of 370–800°C with prominent points at 541.42 and 775.50°C, resulted in the removal of C₅H₈ClN₃O, leading to a reduction in mass of 33.24% (calculated as 33.69%). The remaining product after breakdown was identified as Cadmium oxide (CdO).

Table 4 Thermal Analysis Findings for SB Ligand and Its (ML) complexes via TG and DTG.

Complex	TG-range (°C)	DTG max	n*	Mass loss Estim (calc.%) (Total mass Loss)	Assignment	Residues
[(L) Cr Cl ₃ (H ₂ O)] (C ₁₁ H ₁₄ Cr Cl ₃ N ₆ O ₃)	(20-245)	221.63	1	33.506(33.87)	-Loss of C ₂ H ₇ Cl ₂ N ₂ O ₂	Cr ₂ O ₃
	(245-800)	(352.33,450.45)	2	50.237(50.53)	-Loss of C ₉ H ₇ ClN O ₅	
[(L) Co Cl ₂ (H ₂ O) ₂].2H ₂ O (C ₁₁ H ₂₀ Co Cl ₂ N ₆ O ₆)	(35-160)	98	1	7.50(7.78)	-Loss of 2H ₂ O	CoO
	(160-485)	325	2	57.09(57.57)	-Loss of C ₉ H ₁₃ Cl ₂ N ₃ O ₂	
	(485-800)	85	3	18.22(18.40)	-Loss of C ₂ H ₃ N ₃ O	
[(L) Cu Cl ₂].2H ₂ O (C ₁₁ H ₁₆ Cu Cl ₂ N ₆ O ₄)	(30-150)	96	1	7.832(8.35)	-Loss of 2H ₂ O	CuO
	(150-410)	(227.79,286.44,261.61,386.08)	2	60.223(60.84)	-Loss of C ₉ H ₁₁ Cl ₂ N ₄ O	
	(410-800)	494.43	3	12.414(12.76)	-Loss of C ₂ H ₂ N ₂	
[(L) Cd Cl ₂ (H ₂ O) ₂] (C ₁₁ H ₁₆ Cd Cl ₂ N ₆ O ₄)	(35-210)	120.17,198.69	1	7.03(7.50)	-Loss of 2H ₂ O	CdO
	(210-370)	247.266	2	31.75(32.02)	-Loss of C ₆ H ₄ N ₃ Cl	
	(370-800)	541.42, 775.50	3	33.24(33.69)	-Loss of C ₅ H ₈ ClN ₃ O	

3.3. Geometry optimization

3.3.1. Exploring Molecular Structure and Reactivity Descriptors: A Density Functional Theory Investigation into Computational Insights

The molecular geometry was optimized using Density Functional Theory (DFT), specifically focused on the SB ligand and its Cd (II) complex, which was selected because of its historically considerable biological activity [52]. The optimized geometries with atomic numbering are displayed in Table 6. As presented in Table 7 [53], the bond lengths and angles demonstrate a deformed octahedral geometry surrounding the Cd (II) ion. Supplementary Table 1 contains detailed information about the SB ligand and its Cd (II) complex, including measurements of bond lengths and angles. The Cd (II) complex exhibits slight elongation in some bond lengths, including C (15)-O (18), C(15)-C(16), N(14)-C(15), C(11)-N(13), and N(13)-N(14). The elongation is ascribed to the SB ligand coordinating through the participation of the azomethine nitrogen atom and the oxygen atom of the (C=O) group. The HOMO–LUMO energy gap (ΔE), ionization potential (I), electron affinity (A), chemical potentials (Pi), absolute electronegativity (χ), absolute softness (σ), global electrophilicity (ω), absolute hardness (η), global softness (S), and additional electronic charge (ΔN_{max}) were calculated for both the SB ligand and its Cd(II) complex using consistent computational methods. Table 6 [54] contains comprehensive results. The calculation of these molecular properties requires precise computations, including absolute hardness (η), global softness (S), chemical potential (μ), and electronegativity (χ). The calculation of the HOMO–LUMO energy gap (ΔE) involves subtracting the energy of the LUMO (ELUMO) from the energy of the HOMO (EHOMO). The absolute softness (σ) is determined by taking the reciprocal of the parameter η . The increased electronic charge (ΔN_{max}) is given by the negative value of the parameter I divided by η . A diminished energy gap signifies the existence of charge transfer interactions within the molecule, which impact its biological activity. The energy gap is a significant determinant of a molecule's chemical reactivity. A narrow frontier orbital gap indicates increased reactivity, categorizing the molecule as "soft." The energy gap is a crucial measure of stability, providing insights into the structural and conformational obstacles present in different molecular systems. The energy gap for the SB ligand was found to be 4.781eV, whereas its Cd (II) complex was measured to be 3.70eV. A more

significant energy gap indicates more stability of the molecule. In addition, the chemical potential (μ) had a negative value, whereas the electrophilicity index (χ) had a positive value. These data indicate that the Schiff base ligand will likely act as an electron donor to the metal ions [55]. Table 6 presents a computational investigation of the properties of molecular orbitals. Utilization of Density Functional Theory (DFT) methodology to analyze a binary Cadmium (II) complex and its SB ligand.


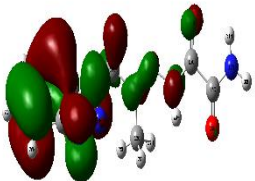
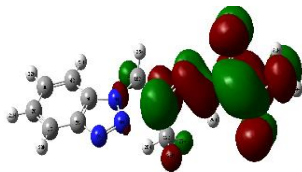
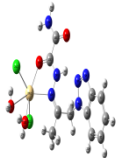
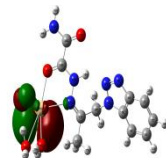
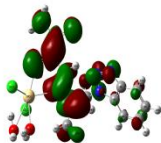
Optimized geometry visualization of the studied SB ligand and its binary Cd(II) Complex				
Compound	optimized structure	3D-HOMO	3D-LUMO	ΔE (eV)
SB ligand				
		$E_{HOMO} = -8.188\text{eV}$	$E_{LUMO} = -1.2691\text{eV}$	4.781
[(L) Cd Cl ₂ (H ₂ O) ₂]				
		$E_{HOMO} = -6.490465025\text{eV}$	$E_{LUMO} = -2.78617606\text{eV}$	3.704

TABLE 7. Comparative Examination of Optimized Quantum Chemical Parameters for an SB ligand and its Binary Cadmium (II) Complexes

Quantum Chemical Parameters Computation	SB ligand	[(L) Cd Cl ₂ (H ₂ O) ₂]
E (a.u)	-905.158876	-1136.16061813
Dipole moment (Debye)	4.1637	9.9091
E_{HOMO} (eV)	-6.829519168	-6.490465025
E_{LUMO} (eV)	-2.04793	-2.78617606
ΔE (eV)	4.781589168	3.704288965
χ (eV)	4.438724584	4.638320543
η (eV)	2.390794584	1.852144482
σ (eV) ⁻¹	0.418270983	0.539914682
μ (eV)	-4.438724584	-4.638320543
S (eV) ⁻¹	0.209135491	0.269957341
ω (eV)	4.120445158	5.807866951
ΔN_{max}	1.856589694	2.504297363
Bond lengths (Å)	SB ligand	[(L) Cd Cl ₂ (H ₂ O) ₂]
C (15)-O (18)	1.250	1.266
C (15)-C (16)	1.547	1.534
N (14)-C (15)	1.372	1.357
C (11)-N (13)	1.303	1.306
N (13)-N (14)	1.388	1.412

Bond angles (o)	SB ligand	[(L) Cd Cl2 (H2O)2]
O (24)-Cd (20)-O (23)	39.772
O (24)-Cd (20)-Cl (22)	115.367
O (24)-Cd (20)-Cl (21)	52.918
O (24)-Cd (20)-O (18)	137.98
O (24)-Cd (20)-N (13)	116.12
O (23)-Cd (20)-Cl (22)	84.938
O (23)-Cd (20)-Cl (21)	92.683
O (23)-Cd (20)-O (18)	160.438
O (23)-Cd (20)-N (13)	96.216
Cl (22)-Cd (20)-Cl (21)	142.149
Cl (22)-Cd (20)-O (18)	105.6
Cl (22)-Cd (20)-N (13)	95.209
Cl(21)-Cd(20)-O(18)	88.815
Cl(21)-Cd(20)-N(13)	122.558
O(18)-Cd(20)-N(13)	66.875

3.3.2. Molecular electrostatic potential (MEP)

An investigation was conducted to analyze the electrostatic potential $V(r)$ maps to determine the electronic charge distribution across the molecule surface while studying molecular reactions. This research aims to forecast possible reaction sites. Using the identical basis set that was optimized by Gaussian software, we obtained 3D Molecular Electrostatic Potential (MEP) maps for both the SB ligand and its Cd (II) complex (see Figure 4).

The MEP analysis generally assigns red color to electron-rich regions, indicating their suitability for electrophilic attack. Conversely, blue portions reflect electron-deficient regions, suggesting their affinity for nucleophilic attack. Green regions indicate a state of electrostatic potential that is neither positive nor negative.

The ligand has a stable charge density that is evenly distributed, except for the sulfur atoms.

These sulfur atoms are surrounded by a more extensive negatively charged area, which suggests they are prone to being attacked by electrophiles. This is highlighted in yellow in Figure 2A. The aromatic ring exhibits a state of electron density that is seemingly neutral.

The electrostatic potential distribution has a considerable impact on complexation reactions. This assertion is substantiated by analyzing the electrostatic potential distribution of the Cd (II) complex, which indicates that the most significant negative charge encompasses the metal center (see Figure 2 B).

The Cd (II) complex demonstrates an enhanced electron-withdrawing ability in sulfur and nitrogen relative to the unbound ligand, rendering these sites more conducive to electrophilic assault. The Mulliken electron-negative study confirms that these areas are the preferred sites for interaction with the metal ion, as shown in Figure 2 [56, 57].

3.4. pharmacology study

The advancements in bio-inorganic chemistry have sparked a growing fascination with SB complexes, which are now acknowledged for their capacity to mimic biologically significant compounds.

Hence, we shall proceed to disclose our discoveries regarding these complexes.

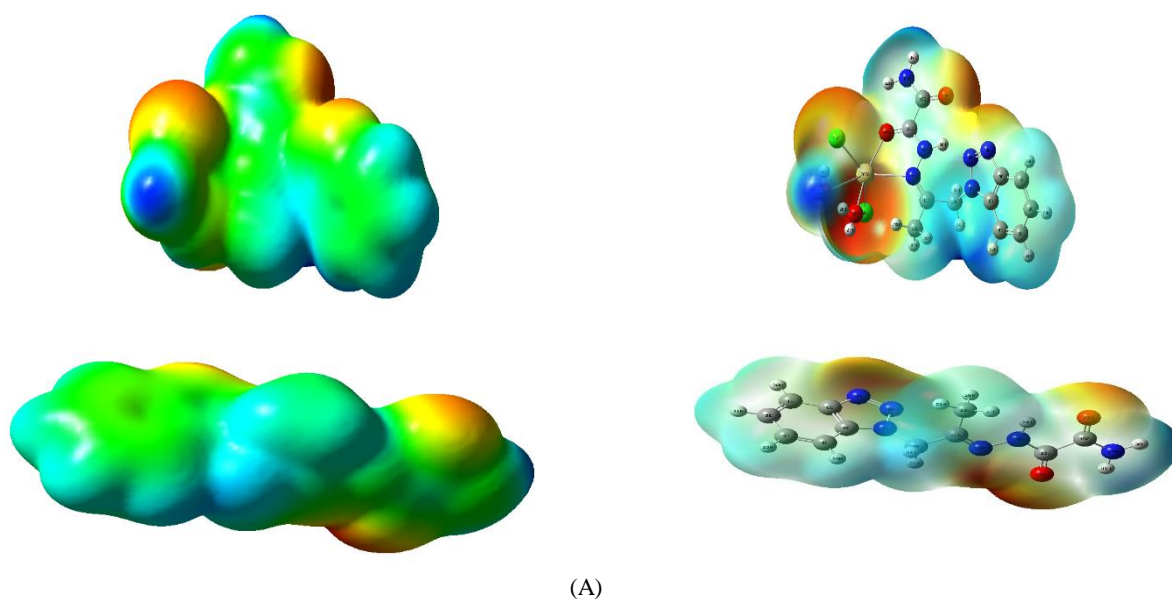


Fig 2. Molecular Electrostatic Potential Mapping for (A) an SB ligand and (B) its Cadmium Complex $[(L) Cd Cl_2 (H_2O)_2]$: Analysis at an Electron Density Iso-surface of 0.004 Atomic Units.

3.4.1 Antimicrobial Efficacy

Experiments were conducted to assess the efficacy of the SB ligand and its metal complex against four distinct bacterial species: *Staphylococcus aureus*, *Streptococcus mutans*, *Escherichia coli*, and *Klebsiella pneumoniae*. Furthermore, a screening procedure was carried out to examine the fungal strains *Candida albicans* and *Aspergillus Nigar* [58]. To assess their biological activity, the SB ligand and its complexes were compared to the antibacterial drugs Gentamicin and Ampicillin and the antifungal medication Nystatin [59]. The metal complexes of chromium (III), cobalt (II), copper (II), and cadmium (II) derived from the Triazole Schiff base demonstrated noteworthy antibacterial efficacy, with the cadmium (II) complex displaying exceptionally high activity. The combination exhibited the most potent antibacterial activity against bacterial species and fungi, as evidenced in Table 10. The importance of this unique attribute of the analyzed triazole Schiff base complexes resides in their capacity to effectively cure infections generated by any of these particular strains [60]. The antibacterial effects of Triazole Schiff base and its binary metal complex were assessed against microorganisms utilizing the disc diffusion technique.

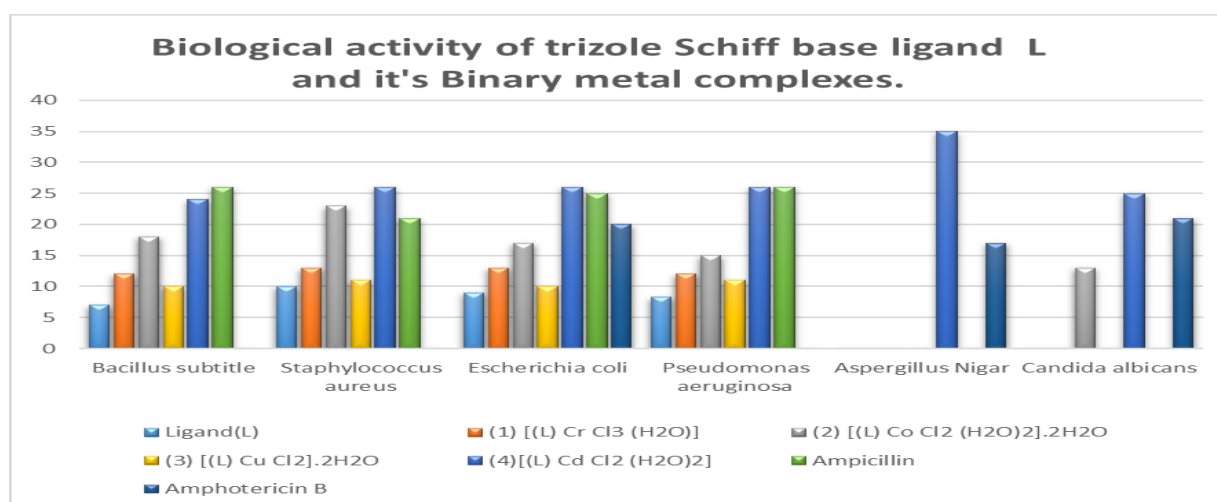
The results indicate that the metal complex has antibacterial characteristics and shows more potent inhibitory activity than the original ligand under experimental circumstances. The antibacterial action has been explained using the chelation theory. Moreover, the results indicated that the tested complexes were more effective against Gram-positive than Gram-negative bacteria. The antibacterial action of the chemicals is intimately correlated with the composition and arrangement of the bacteria's cell wall. It is widely recognized that Gram-negative bacteria have lipopolysaccharides in their outer membrane. The synthetic Schiff base and its metal complex can interact with the hydrophobic layer, enhancing the membrane permeability of Gram-negative bacteria. The cell is enclosed by a lipid barrier that selectively permits only lipid-soluble compounds to pass through.

This means that the ability to dissolve in lipids is essential in determining antimicrobial action's effectiveness. Moreover, the increase in lipophilicity enhances the capacity of the Schiff base and its metal complex to penetrate the lipid membranes, hindering the organism's subsequent growth. The cell wall plays a vital role in the survival of many bacteria, and many antibiotics can eradicate bacteria by impeding a particular step in the synthesis of peptidoglycan [60]. The compounds are classified based on their specific effects. The metal ions can be arranged in decreasing order of reactivity with the ligand as follows: $Cd(II) > Co(II) > Cr(III) > Cu(II)$.

The heightened activity of the metal complex can be ascribed to the impact of metal ions on the conventional cell membrane. Metal chelates have polar and nonpolar properties, making them very suitable for penetrating cellular and tissue structures. Moreover, chelation has the potential to either enhance or diminish the metabolic capacities of bioactive organic compounds [61]. Cadmium (II) exhibited the highest activity, whereas the ligand and copper (III) complexes demonstrated the lowest level. The antifungal activity of Cd (II) complexes exceeds the standard. The precise outcomes of these assessments are displayed in Table 8 and graphically depicted in Figure 3.

Table 8. Exploring the Bioactivity of an SB ligand and Its Metal C0mplex: An Investigation into Biological Effects.

Sample	Inhibition zone diameter (mm/mg sample)					
	Gram-positive bacteria		Gram-negative bacteria		Fungi	
	<i>Bacillus subtilis</i>	<i>Staphylococcus aureus</i>	<i>Escherichia coli</i>	<i>Pseudomonas aeruginosa</i>	<i>Aspergillus Nigar</i>	<i>Candida albicans</i>
Control: DMSO	0	0	0	0	0	0
Ligand(L)	7±0.5	10±0.5	9±1	8.3±0.1	NA	NA
[(L) Cr Cl3 (H2O)]	12±0.5	13±0.6	13±0.6	12	NA	NA
[(L) Co Cl2 (H2O)2].2H2O	18±0.5	23±0.5	17±0.1	15±0.5	NA	13 ±0.5
[(L) Cu Cl2].2H2O	10±0.5	11±0.5	10±0.5	11±0.5	NA	NA
[(L) Cd Cl2 (H2O)2]	24±0.6	26±0.5	26±0.5	26±1.0	35.0±1.0	25±0.5
Ampicillin	26	21	25	26	-----	-----
Amphotericin B	-----	-----	-----	-----	17	21

**Fig 3.** Evaluation of the Biological Activity of triazole SB ligand and Its (ML) C0mplex

3.4.2. Anticancer activities

Cancer, also known as malignant neoplasms, refers to illnesses involving abnormal cell growth, invasive activity, and, in some instances, the ability to spread to other body parts [62]. It remains a major global health problem, remaining the most feared diagnosis. After cardiovascular illnesses, it is the second most common cause of death in both developing and industrialized countries [63].

Currently, the primary treatment strategy for cancer mainly involves surgical procedures and chemotherapy. Nevertheless, the effectiveness of existing chemotherapeutic medicines is not ideal, and they are often associated with a wide range of adverse side effects. Over the past five decades, there has been a strong emphasis on developing more powerful medications to combat cancer. Other variations of SBs have recently emerged as exciting candidates demonstrating anti-cancer capabilities. Within the domain of laboratory experimentation, *in vitro* studies were conducted to assess the cytotoxic

effects of a ligand and its complexes on MCF-7 (Breast cancer) cells. Survival curves were generated to illustrate the relationship between the concentration of the chemicals and the relative viability of cells. Please refer to Figure 4 for further details. Furthermore, Table 9 provides IC50 values, which indicate the dose at which there is a 50% inhibition of cancer cell growth. The key findings on the toxicity against MCF-7 cells are briefly presented as follows:

TABLE 9: Anticancer Efficacy Targeting Breast Cancer: Evaluation of triazole SB ligand and Its binary Metal C0mplex

ID	Conc. ug/ml	O.D			Mean O.D	ST.E	Viability %	Toxicity %	IC50
Mcf7	-----	0.603	0.614	0.595	0.604	0.005508	100	0	
	1000	0.018	0.017	0.019	0.018	0.000577	2.98013245	97.01986755	
Triazole Schiff base Ligand	500	0.02	0.017	0.021	0.019333	0.001202	3.200883002	96.799117	
	250	0.192	0.156	0.188	0.178667	0.011392	29.58057395	70.41942605	172.57
	125	0.327	0.352	0.331	0.336667	0.007753	55.73951435	44.26048565	
	62.5	0.482	0.536	0.517	0.511667	0.015815	84.71302428	15.28697572	
	31.25	0.599	0.609	0.6	0.602667	0.00318	99.77924945	0.220750552	
1000	0.014	0.016	0.017	0.015667	0.000882	2.593818985	97.40618102		
[(L) Cr Cl3 (H2O)]	500	0.016	0.018	0.016	0.016667	0.000667	2.759381898	97.2406181	
	250	0.074	0.089	0.063	0.075333	0.007535	12.47240618	87.52759382	
	125	0.112	0.153	0.137	0.134	0.01193	22.18543046	77.81456954	
	62.5	0.284	0.288	0.293	0.288333	0.002603	47.73730684	52.26269316	77.99
	31.25	0.563	0.529	0.548	0.546667	0.009838	90.50772627	9.492273731	
	1000	0.015	0.017	0.014	0.015333	0.000882	2.538631347	97.46136865	
[(L) Co Cl2 (H2O)2].2H2O	500	0.019	0.017	0.02	0.018667	0.000882	3.090507726	96.90949227	
	250	0.093	0.142	0.116	0.117	0.014154	19.37086093	80.62913907	86.67
	125	0.193	0.216	0.202	0.203667	0.006692	33.7196468	66.2803532	
	62.5	0.316	0.299	0.358	0.324333	0.017534	53.69757174	46.30242826	
	31.25	0.472	0.529	0.505	0.502	0.016523	83.11258278	16.88741722	
1000	0.019	0.02	0.018	0.019	0.000577	3.145695364	96.85430464		
[(L) Cu Cl2].2H2O	500	0.022	0.02	0.018	0.02	0.001155	3.311258278	96.68874172	
	250	0.023	0.028	0.033	0.028	0.002887	4.635761589	95.36423841	
	125	0.031	0.037	0.035	0.034333	0.001764	5.684326711	94.31567329	72.54
	62.5	0.242	0.289	0.274	0.268333	0.01386	44.42604857	55.57395143	
	31.25	0.588	0.602	0.601	0.597	0.004509	98.8410596	1.158940397	
	1000	0.017	0.014	0.017	0.016	0.001	2.649006623	97.35099338	
[(L) Cd Cl2 (H2O)2]	500	0.018	0.016	0.018	0.017333	0.000667	2.869757174	97.13024283	
	250	0.019	0.022	0.026	0.022333	0.002028	3.697571744	96.30242826	
	125	0.032	0.027	0.041	0.033333	0.004096	5.518763797	94.4812362	
	62.5	0.1	0.094	0.119	0.104333	0.007535	17.27373068	82.72626932	36.14
	31.25	0.327	0.293	0.313	0.311	0.009866	51.49006623	48.50993377	

- A) The IC₅₀, measured in µg/ml, indicates the drug concentration needed to prevent 50% of cancer cell growth. This value is a reliable indicator of the substance's ability to cause cell death.
- B) B) The IC₅₀ spectrum, measured in micrograms per milliliter (µg/ml), categorizes the effectiveness of the drug into specific ranges: 1-10 (high potency), 11-20 (potent), 21-50 (moderate potency), 51-100 (mild potency), and above 100 (non-cytotoxic) [68]. Specifically, the focus is on MCF-7, a breast cancer cell line subtype.

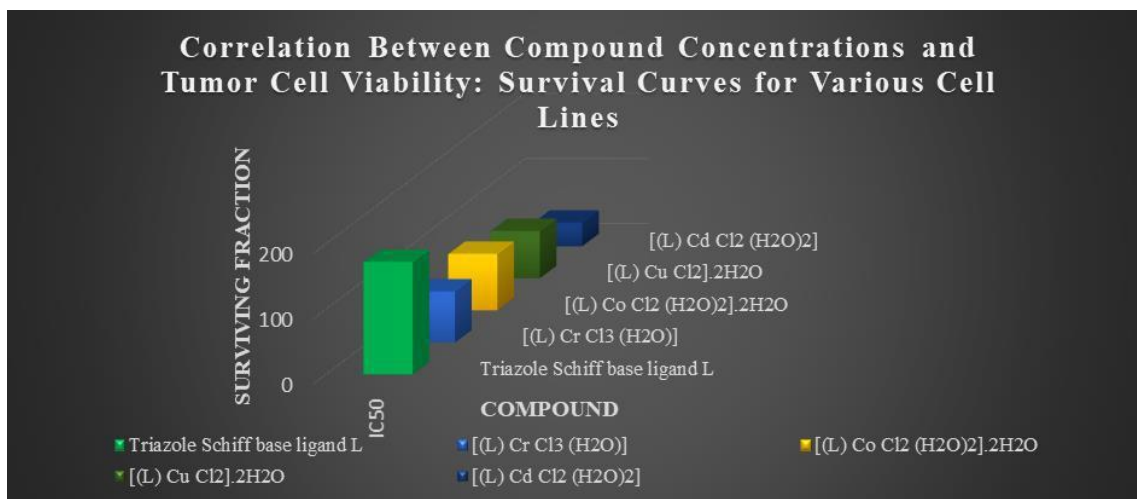


Fig 4. Anticancer Efficacy on Breast Cancer of triazole SB ligand and Its Binary Metal Complex

3.5. Docking study of triazole SB ligand and its binary [(L) Cd Cl₂ (H₂O)₂] complex.

An inquiry was commenced to examine possible locations where a Schiff base ligand triazole (referred to as L) and its binary Cadmium (II) complex can bind within three separate receptor entities (2JFZ, 3QX3, and 6XBH). The first receptor (PDB ID: 2JFZ) represents *Helicobacter pylori* glutamate racemase crystal structure in conjunction with D-Glutamate and an inhibitor. The second receptor, with the PDB ID 3QX3, describes the crystal structure of Human topoisomerase IIbeta in a complex formation with DNA and etoposide. The third receptor, with the Protein Data Bank (PDB) ID 6XBH, represents the crystal structure of the primary protease of the SARS-CoV-2 virus (responsible for COVID-19) when it is bound to the inhibitor UAW247. The computational research utilized the MOE 2014.09 software platform to accurately predict the binding interaction modes occurring within the interior pockets on the protein surface. The computations were executed on a computer system featuring an Intel Pentium 1.6-GHz central processing unit and 8 gigabytes of random access memory, operating on the Windows 10 operating system. The minimization technique was performed using MOE until an RMSD gradient of 0.05 KCal/mol Å was attained. The MMFF94X force field was utilized, and automated calculations of partial charges were included. The docking data for the triazole Schiff base ligand (referred to as "L") and its binary Cd (II) complex are displayed in both two-dimensional (2D) and three-dimensional (3D) visualizations, as outlined in Table 12. Table 10 contains data regarding the binding energies of the triazole SB ligand, whereas Table 11 presents information on the binding energies of its binary Cd (II) complex.

Experimental results indicate that the triazole Schiff base ligand, referred to as L, had a noteworthy IC₅₀ value of 172.57 µg/ml when evaluated against a breast cancer cell line. The binary Cadmium (II) complex, [(L) Cd Cl₂ (H₂O)₂], derived from the previously mentioned triazole ligand, had enhanced efficacy against cancer, as seen by its reduced IC₅₀ values of 36.14 µg/ml. In theory, docking studies were conducted to substantiate these findings, particularly on three receptors. The initial receptor of interest is the Crystal structure of *Helicobacter pylori* glutamate racemase in association with D-Glutamate and an inhibitor, identified by the PDB ID: 2JFZ. The Glutamate racemase, a vital enzyme involved in synthesizing bacterial cell walls, is considered a promising target for developing antibacterial medications. The docking research findings indicated that the triazole SB ligand exhibited a binding energy of -2.7 kcal mol⁻¹, whereas its binary Cadmium (II) complex demonstrated a binding energy of -4.3 kcal mol⁻¹. This signifies enhanced reactivity of the complexes compared to the original ligand, resulting from forming coordination bonds with the Cadmium (II) metal ion. In addition, docking investigations were conducted utilizing the Crystal structure of Human topoisomerase IIbeta in conjunction with DNA and etoposide (PDB ID: 3QX3). Various anticancer medicines target human topoisomerase IIbeta at the molecular level. The findings revealed notably low binding energies of -2.9 and -23.1 kcal mol⁻¹ for the SB ligand and its Cadmium (II) complex, respectively. This suggests that the complexes exhibit enhanced activity compared to the original ligand, which can be attributed to forming coordination bonds with the Cadmium (II) metal ion. In conclusion, a thorough examination of the interactions between these medications and the protein receptor of SARS-CoV-2 (COVID-19) revealed notable and influential interactions. The main observed interaction forces were hydrogen bonding, ionic bonding, and π-H interactions. The triazole SB ligand and its binary Cd (II) complex, coupled with receptors 2JFZ, 3QX3, and 6XBH, had distinct binding energies. The Schiff base ligand L had the lowest binding energies, measured at -2.7, -2.9, and -1.6 kcal mol⁻¹. Conversely, the Cd (II) complex exhibited binding energies of -4.3, -23.1, and -6.3 kcal mol⁻¹ with the

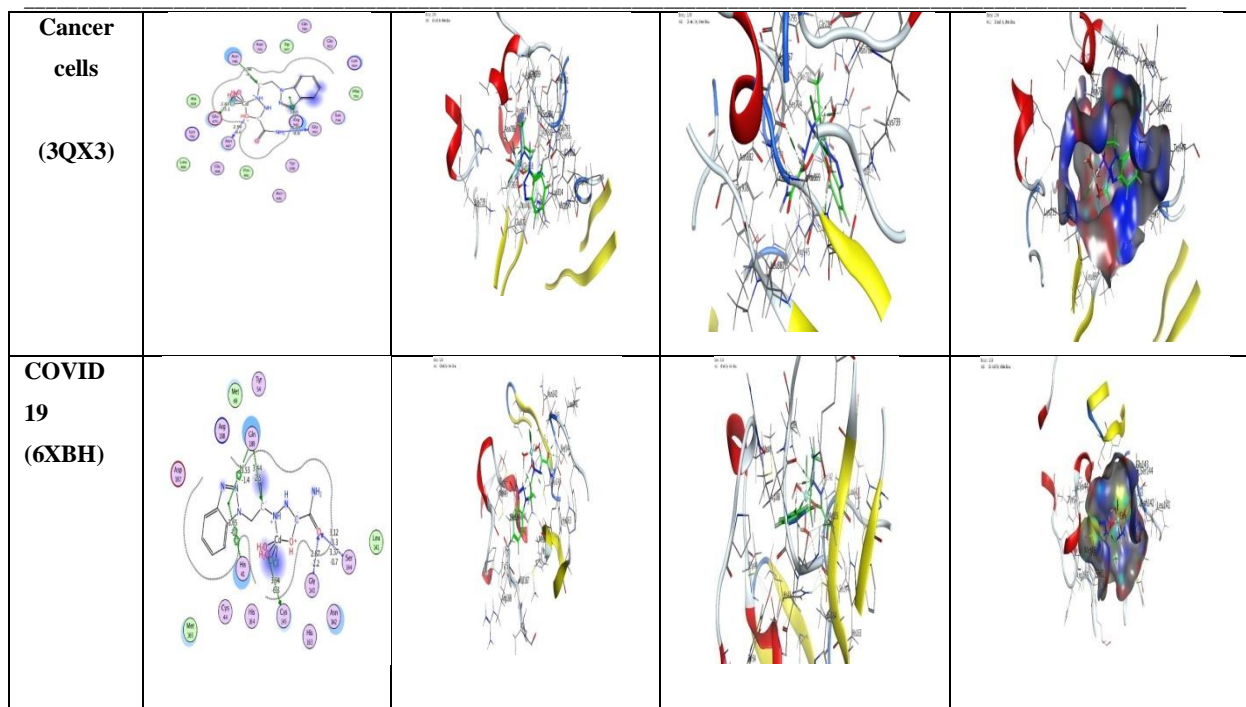
respective receptors. Remarkably, the coordination process resulted in a conspicuous reduction in binding energy. Hence, the Cd (II) complex in binary form showed enhanced activity compared to the triazole Schiff base ligand L. This indicates its potential efficacy as a promising therapeutic agent for treating human illnesses in future applications.

TABLE 10: Calculated Interaction Energies: Docking Assessment of Triazole SB ligand with Diverse Protein Receptors Linked to H-Pylori, Cancer Cells, and COVID-19

Type	Receptor	Ligand moiety	Receptor site	Interaction	Distance (Å°)	E (kcal/mol)
H-Pylori	2JFZ	N 17	OG SER 152 (A)	H-donor	2.95	-2.7
		N 14	O GLY 868 (A)	H-donor	3.62	-0.6
Cancer cells	3QX3	N 17	OE2 GLU 870 (A)	H-donor	2.98	-2.9
		N 17	O LEU 880 (A)	H-donor	3.16	-1.1
		O 19	CA PRO 881 (A)	H-acceptor	3.29	-0.9
		O 19	OH TYR 908 (A)	H-acceptor	2.69	-1.4
		O 19	OG SER 144 (A)	H-acceptor	3.14	-0.7
COVID 19	6XBH	5-ring	NE2 GLN 189 (A)	pi-H	3.57	-1.6

TABLE 11: Evaluating Interaction Energies Arising from Docking Simulations of Binary Cd (II) Complex with Diverse Protein Receptors Linked to H-Pylori, Cancer Cells, and COVID-19.

Type	Receptor	Ligand moiety	Receptor site	Interaction	Distance (Å°)	E (kcal/mol)
H-Pylori	2JFZ	CL 24	OG SER 152 (A)	H-donor	3.09	-2.2
		O 25	O ILE 149 (A)	H-donor	3.25	-4.3
		5-ring	CD2 LEU 186 (A)	pi-H	4.19	-0.6
Cancer cells	3QX3	N 18	O GLY 793 (A)	H-donor	3.05	-0.8
		O 19	O ASN 867 (A)	H-donor	2.99	-9.6
		O 25	OE2 GLU 870 (A)	H-donor	2.63	-23.1
		C 11	ND2 ASN 786 (A)	H-acceptor	2.98	-4.0
		O 25	OE2 GLU 870 (A)	ionic	2.63	-7.5
		5-ring	NH2 ARG 945 (A)	pi-cation	3.66	-3.0
		O 25	SG CYS 145 (A)	H-donor	3.94	-6.3
COVID 19	6XBH	C 11	NE2 GLN 189 (A)	H-acceptor	3.44	-2.5
		O 21	N GLY 143 (A)	H-acceptor	2.87	-2.2
		O 21	N SER 144 (A)	H-acceptor	3.12	-3.3
		O 21	OG SER 144 (A)	H-acceptor	3.37	-0.7
		5-ring	NE2 GLN 189 (A)	pi-H	3.53	-1.4
		5-ring	5-ring HIS 41 (A)	pi-pi	3.65	-0.0



4. Conclusion

This study thoroughly analyzes a bidentate Triazole Schiff base ligand, referred to as Ligand L, and its corresponding binary metal C0mplex. Several analytical methods, such as elemental analysis, molar conductance, mass spectroscopy, ¹H NMR, infrared (IR), and UV-visible spectroscopy, were used to characterize the sample thoroughly. The investigations revealed the development of octahedral-shaped complexes, namely [(L) Cr Cl₃ (H₂O)], [(L) Co Cl₂ (H₂O)₂].2H₂O, and [(L) Cd Cl₂ (H₂O)₂], as well as a square planar-shaped complex [(L) Cu Cl₂]. The chemical formula is H₂O. The antimicrobial assessment revealed that the [(L) Cd Cl₂ (H₂O)₂] binary complex had significantly increased toxicity against both bacterial and fungal species. Furthermore, the study found that the Triazole Schiff base binary metal complex showed significant efficacy against MCF-7, a breast cancer. This suggests that the complex can exhibit a range of biological activities. These findings emphasize the potential of these molecules for further investigation in medical and pharmacological research.

References

1. Vigato, P.A.; Tamburini, S. The cyclic and acyclic Schiff bases and related derivatives challenge. *Coord. Chem. Rev.* 2004, 248,1717–2128.
2. Asghar SF, Yasin KA, Habib-ur-Rehman, Aziz S. Synthesis and cyclisation of 1,4-disubstituted semicarbazides. *Natural Product Research.* 2010 Mar 10;24(4):315–25.
3. Rajesh-Rane A, Shital-Naphade S, Pavan Kumar, Mahesh Palkar B, Mahamadhanif Shaikh S, Rajshekhar Karpoomath. Synthesis of novel 4- tetrapyrrole-based semicarbazide and thiosemicarbazide hybrids with antimicrobial and antitubercular activity. *Bioorganic & Medicinal Chemistry Letters.* 2014 Jul 24;10: 3079-3083.
4. Pituchaa M, Karczmarzykb Z, Kosikowska U, and Malm A. Synthesis, Experimental and Theoretical Study on the Structure of Some Semicarbazides with Potential Antibacterial Activity. *Zeitschriftfür Naturforschung B.* 2011 Apr 66;(5) 971-87.
5. Rafat-Mohareb M. and Abeer Mohamed A. Uses of 1-Cyanoacetyl-4-Phenyl-3-Thiosemicarbazide in the Synthesis of Antimicrobial and Antifungal Heterocyclic Compounds. *International Research Journal of Pure & Applied Chemistry.* 2012 Jul 2(2): 2012 144-155.
6. Da Silva, C.M.; Silva, M.M.; Reis, F.S.; Ruiz, A.L.T.; De Carvalho, J.E.; Santos, J.C.; Figueiredo, I.M.; Alves, R.B.; Modolo, L.V.; De Fátima, Â. Studies on free radical scavenging, cancer cell antiproliferation, and calf thymus DNA interaction of Schiff bases. *J. Photochem. Photobiol. B, Biol.* 2017, 172, 129-138.
7. Zheng, J.; Ma, L. Silver(I) complexes of 2,4-dihydroxybenzaldehyde–amino acid Schiff bases—novel noncompetitive α-glucosidase inhibitors. *Bioorg. Med. Chem. Lett.* 2015, 25, 2156-2161.
8. M.Y. Nassar, T.Y. Mohamed, I.S. Ahmed, One-pot solvothermal synthesis of novel cobalt salicylaldimine-urea complexes: a new approach to Co₃O₄ nanoparticles. *J. Mol. Struct.* 1050, 81–87 (2013).

9. Mohapatra, R. K., Sarangi, A. K., Azam, M., El-ajaily, M. M., Kudrat-E-Zahan, M., Patjoshi, S. B., & Dash, D. C. (2019). Synthesis, structural investigations, DFT, molecular docking, and antifungal studies of transition metal C0mplex with benzothiazole-based Schiff base ligands. *Journal of Molecular Structure*, 1179, 65–75.
10. Van de Loosdrecht, A. A., Beelen, R. H. J., Ossenkoppele, gGJ, Broekhoven, M. G., & Langenhuijsen, M. (1994). A tetrazolium-based colorimetric MTT assay to quantitate human monocyte-mediated cytotoxicity against leukemic cells from cell lines and patients with acute myeloid leukemia. *Journal of Immunological Methods*, 174(1–2), 311–320.
11. Alley, M. C., Scudiero, D. A., Monks, A., Hursey, M. L., Czerwinski, M. J., Fine, D. L., ... Boyd, M. R. (1988). Feasibility of drug screening with panels of human tumor cell lines using a microculture tetrazolium assay. *Cancer Research*, 48(3), 589–601.
12. Slater, T. F., Sawyer, B., & Sträuli, U. (1963). Studies on succinate-tetrazolium reductase systems: III. Points of coupling of four different tetrazolium salts III. Points of coupling of four different tetrazolium salts. *Biochimica et Biophysica Acta*, 77, 383–393.
13. Abdallah, S. M., Zayed, M. A., & Mohamed, G. G. (2010). Synthesis and spectroscopic characterization of new tetradentate Schiff base, its coordination compounds of NOON donor atoms, and their antibacterial and antifungal activity. *Arabian Journal of Chemistry*, 3(2), 103–113.
14. Radwan, M. T., Mahmoud, W. H., ElMosallamy, M. A. F., & El-Sherif, A. A. (2023). TRANSITION METAL COMPLEX INCORPORATING SYMMETRIC tetra dentate Schiff base ligand: Synthesis, characterization, biological activities, DFT and molecular docking studies. *Egyptian Journal of Chemistry*, 66(13), 1329–1339.
15. Frisch, M.J., Trucks, G.W., Schlegel, H.B., Scuseria, G.E., Robb, M.A., Cheeseman, J.R. Gaussian 09, Revision A.02, Gaussian Inc, Wallingford CT 34, Wallingford CT (2009).
16. Dennington, R. D., Keith, T. & Millam, J. GaussView, Version 4.1. 2 (SemicheM Inc., Shawnee Mission, KS, 2007).
17. Becke, A. D. A new mixing of Hartree-Fock and local density-functional theories. *J. Chem. Phys.* 98, 1372–1377. [https://doi.org/ 10.1063/1.464304](https://doi.org/10.1063/1.464304) (1993).
18. El-gharry, M. A., Elzawawi, F. M., Aziz, A. A. A., Nassir, K. M. & Abu-El-Wafa, S. M. New Schiff base ligand and its novel Cr (III), Mn (II), Co (II), Ni (II), Cu (II), Zn (II) complexes: Spectral investigation, biological applications, and semiconducting properties. *Sci. Rep.* 12, 17942. <https://doi.org/10.1038/s41598-022-22713-z> (2022).
19. A. W. Bauer, W. M. Kirby, J. C. Sherris, M. Turck, *Am. J. Clin. Pathol.* 1966, 45, 493–496.
20. Y. M. Ahmed, W. H. Mahmoud, M. M. Omar, G. G. Mohamed, *J. Inorg. Organomet. Polym. Mater.* 2021, 31, 2339–2359.
21. A. W. Bauer, W. M. Kirby, J. C. Sherris, M. Turck, *Am. J. Clin. Pathol.* 1966, 45, 493–496.
22. Scott, A. C. (1989). Laboratory control of antimicrobial therapy. *Practical Medical Microbiology*, 13, 161–181.
23. Skehan, P., Strong, R., Scudiero, D., Monks, A., McMahon, J., Vistica, D., Warren, J. T., Bokesch, H., Kenney, S., & Boyd, M. R. (1990). New colorimetric cytotoxicity assay for anticancer-drug screening. *JNCI: Journal of the National Cancer Institute*, 82(13), 1107–1112.
24. Lundqvist, T., Fisher, S. L., Kern, G., Folmer, R. H. A., Xue, Y., Newton, D. T., Keating, T. A., Alm, R. A., & de Jonge, B. L. M. (2007). Exploitation of structural and regulatory diversity in glutamate racemases. *Nature*, 447(7146), 817–822.
25. Etoposide, A. D. (2005). Stru ctural Basis of Type II Topoisomerase Inhibition by the. *Proc. Natl. Acad. Sci. USA*, 102, 3703.
26. Sacco, M. D., Ma, C., Lagarias, P., Gao, A., Townsend, J. A., Meng, X., Dube, P., Zhang, X., Hu, Y., & Kitamura, N. (2020). Structure and inhibition of the SARS-CoV-2 main protease reveal a strategy for developing dual inhibitors against Mpro and cathepsin L. *Science Advances*, 6(50), eabe0751.
27. C. Balakrishnan, L. Subha, M. A. Neelakantan, S. S. Mariappan, *Spectrochim. Acta A.* 2015, 150, 671.
28. M. S. Mansour, W. H. Mahmoud, and A. A. El- Sherif, “Manganese, Cobalt, and Cadmium Complexes of Quinazoline Schiff Base Ligand and Methionine: Synthesis, Characterization, DFT, Docking studies and biomedical application,” *Egypt. J. Chem.*, 2024.
29. M. S. A. Mansour, A. A. El-Sherif, W. H. Mahmoud, and AbeerTaha, “QCM-Based Nano Schiff base Quinazoline-methionine hybrid ligand complex with Cobalt (II) as a Fast Response Nanosensor for instantaneous Monitoring water pollutant Pb(II) Ions,” *Egypt. J. Chem.*, 2024.
30. E.M. Zayed, E.H. Ismail, G.G. Mohamed, M.M.H. Khalil, A.B. Kamel, Synthesis, spectroscopic and structural characterization, and antimicrobial studies of metal C0mplex of a new hexadentate Schiff base ligand. Spectrophotometric Fe (III) determination in water samples using a recovery test. *Monatsh. Chem.* 2014, 145, 755–765.
31. Frisch, A., Nielson, A. B., & Holder, A. J. (2000). Gaussview user manual. Gaussian Inc., Pittsburgh, PA, 556.

32. Annaraj, B., Pan, S., Neelakantan, M. A., & Chattaraj, P. K. (2014). DFT study on the ground state and excited state intramolecular proton transfer of propargyl arm containing Schiff bases in solution and gas phases. *Computational and Theoretical Chemistry*, 1028, 19–26.
33. M. Hanif, Z.H. Chohan, *Spectrochim. Acta A*, 2013, 104, 468–476.
34. M. Hanif, Z.H. Chohan, *Spectrochim. Acta A*, 2013, 104, 468–476.
35. A.M.A. Alaghaz, H.A. Bayoumi, Y.A. Ammar, S.A. Aldhlmani, *J. Mol. Str.*, 2013, 1035, 383–399,
36. İlhan, S. (2009). Synthesis and spectral studies of new macrocyclic Schiff base Cu (II), Ni (II), Cd (II), Zn (II), Pb (II), and La (III) complexes containing pyridine head unit. *Russian Journal of Coordination Chemistry*, 35(5), 347–351.
37. M.Anu*, P.Lakshmi Prabha, G.Banukarathi, P.Rexy Kanjana, K.Rajeshwari“UV-VISIBLE, IR AND NMR SPECTRA ON COPPER (II) SCHIFF BASE COMPLEX ” International Standard Serial Number (ISSN): 2249-6807 *International Journal of Institutional Pharmacy and Life Sciences* 3(6), 23 - 32: November–December 2013.
38. Mohammadi, K., Azad, S. S., & Amoozegar, A. (2015). New tetradentate Schiff bases of 2-amino-3, 5-dibromobenzaldehyde with aliphatic diamines and their metal C0mplex: Synthesis, characterization and thermal stability. *Spectrochimica Acta Part A: Molecular and Biomolecular Spectroscopy*, 146, 221–227.
39. V.LDorofeev, *Pharm. Chem. J*; 2004, 38: 45-49.
40. M.S. Refat, G.G. Mohamed, R.F. Farias, A.K. Powell, M.S. El-Garib, S.A. El-Korashy, M.A. Hussien, *J. Therm. Anal. Calor.*, 2010, 102: 225–232.
41. L.J. Bellamy, *The Infrared Spectra of Complex Molecules*, third ed., Chapman and Hall, London, , 1975.
42. K.D. Patel, H.S. Patel, *Arab. J. Chem.*, 2013, article in press.
43. Abou-Hussein, A. A., & Linert, W. (2014). Synthesis, spectroscopic, coordination and biological activities of some organometallic complexes derived from thio-Schiff base ligands. *Spectrochimica Acta Part A: Molecular and Biomolecular Spectroscopy*, 117, 763–771.
44. Arafath, M. A., Adam, F., Razali, M. R., Hassan, L. E. A., Ahamed, M. B. K., & Majid, A. M. S. A. (2017). Synthesis, characterization and anticancer studies of Ni (II), Pd (II) and Pt (II) complexes with Schiff base derived from N-methylhydrazinecarbothioamide and 2-hydroxy-5-methoxy-3-nitrobenzaldehyde. *Journal of Molecular Structure*, 1130, 791–798.
45. Mahmoud, W. H., Mahmoud, N. F., & Mohamed, G. G. (2017). New nanobidentate Schiff base ligand of 2-aminophenol with 2-acetyl ferrocene with some lanthanide metal ions: synthesis, characterization and Hepatitis A, B, C and breast cancer docking studies. *Journal of Coordination Chemistry*, 70(20), 3552–3574.
46. Kumar, S., Dhar, D. N., & Saxena, P. N. (2009). Applications of metal C0mplex of Schiff bases-A review.
47. Tümer, M., Ekinçi, D., Tümer, F., & Bulut, A. (2007). Synthesis, characterization and properties of some divalent metal (II) complexes: Their electrochemical, catalytic, thermal and antimicrobial activity studies. *Spectrochimica Acta Part A: Molecular and Biomolecular Spectroscopy*, 67(3–4), 916–929.
48. Balasubramanian, K. P., Parameswari, K., Chinnusamy, V., Prabhakaran, R., & Natarajan, K. (2006). Synthesis, characterization, electro chemistry, catalytic and biological activities of ruthenium (III) complexes with bidentate N, O/S donor ligands. *Spectrochimica Acta Part A: Molecular and Biomolecular Spectroscopy*, 65(3–4), 678–683.
49. Baošić, R., Radojević, A., Radulović, M., Miletić, S., Natić, M., & Tešić, Ž. (2008). Relationships between structure, retention and biological activity of some Schiff base ligands and their complexes. *Biomedical Chromatography*, 22(4), 379–386.
50. Kumar, K. S., & Aravindakshan, K. K. (2021). Synthesis, cytotoxic, anticancer and antimicrobial activities of some metal C0mplex of a novel tetradentate Schiff base ligand,(E)-3-((2-((E)-(1-(2-hydroxyphenyl) ethylidene) amino) ethyl) imino)-N-phenylbutanamide. *Results in Chemistry*, 3, 100129.
51. Jain, A. K., Singh, R. K., Jain, S., & Raison, J. (2008). Copper (II) ion selective electrode based on a newly synthesized Schiff-base chelate. *Transition Metal Chemistry*, 33, 243–249.
52. Schlegel, H. B. (1982). Optimization of equilibrium geometries and transition structures. *Journal of Computational Chemistry*, 3(2), 214–218.
53. Tyagi, P., Tyagi, M., Agrawal, S., Chandra, S., Ojha, H., & Pathak, M. (2017). Synthesis, characterization of 1, 2, 4-triazole Schiff base derived 3d-metal C0mplex: Induces cytotoxicity in HepG2, MCF-7 cell line, BSA binding fluorescence and DFT study. *Spectrochimica Acta Part A: Molecular and Biomolecular Spectroscopy*, 171, 246–257.
54. Abdou, A.; Hassan, M.M.; Abdel-Mawgoud, M. Seven metal-based bi-dentate NO azocoumarine complexes: Synthesis, physicochemical properties, DFT calculations, drug-likeness, in vitro antimicrobial screening and molecular docking analysis. *Inorg. Chim. Acta* 2022, 539, 121043.
55. Ali El-Remaily, M.A.E.A.A.; El-Dabea, T.; Alsawat, M.; Mahmoud, M.H.; Alfi, A.A.; El-Metwaly, N.; Abu-Dief, A.M. Development of new thiazole complexes as powerful catalysts for synthesis of pyrazole-4-carbonitrile derivatives under ultrasonic irradiation condition supported by DFT studies. *ACS Omega* 2021, 6, 21071–21086.
56. R. K. Mohapatra, S. Mishra, M. Azam, K. Dhama, De Gruyter. 2021, 16, 491–493.

57. R. Sahu, R. K. Mohapatra, S. I. Al-Resayes, D. Das, P. K. Parhi, S. Rahman, L. Pintilie, M. Kumar, A. Ansari, J. Saudi Chem. Soc. 2021, 25, 101193.
58. H. F. Abd El-Halim, G. G. Mohamed, J. Mol. Struct. 2016, 1104, 91–5.
59. W. H. Mahmoud, N. F. Mahmoud, G. G. Mohamed, A. A. El-Bindary, A. Z. El-Sonbati, J. Mol. Struct. 2015, 1086, 266–75.
60. El-Sherif A.A., Eldebss T.M.A. Synthesis, spectral characterization, solution equilibria, in vitro antibacterial and cytotoxic activities of Cu(II), Ni(II), Mn(II), Co(II) and Zn(II) complexes with Schiff base derived from 5-bromosalicylaldehyde and 2-aminomethylthiophene. Spectrochim Acta.
61. Nair M.S., Arish D., Joseyphus R.S. Synthesis, characterization, antifungal, antibacterial and DNA cleavage studies of some heterocyclic Schiff base metal complex. J Saud Chem Soc. 2012;16:83–88.
62. DeVita, V. T., Lawrence, T. S., & Rosenberg, S. A. (2008). DeVita, Hellman, and Rosenberg's cancer: principles & practice of oncology (Vol. 2). Lippincott Williams & Wilkins.
63. Bandgar, B. P., Gawande, S. S., Bodade, R. G., Totre, J. V., & Khobragade, C. N. (2010). Synthesis and biological evaluation of simple methoxylated chalcones as anticancer, anti-inflammatory and antioxidant agents. Bioorganic & Medicinal Chemistry, 18(3), 1364–1370.
64. Zafar, H., Kareem, A., Sherwani, A., Mohammad, O., Ansari, M. A., Khan, H. M., & Khan, T. A. (2015). Synthesis and characterization of Schiff base octaazamacrocyclic complexes and their biological studies. Journal of Photochemistry and Photobiology B: Biology, 142, 8–19.
65. Khan, T. A., Naseem, S., Hajra, R., & Shakir, M. (2010). Synthesis, Physicochemical, and Antimicrobial Screening Studies of Complexes of Co (II), Ni (II), Cu (II), and Zn (II) with 18-membered Schiff Base Octaazamacrocyclic Ligand. Synthesis and Reactivity in Inorganic, Metal–Organic, and Nano-Metal Chemistry, 40(10), 861–868.
66. Cotton, F. A., Wilkinson, G., Murillo, C. A., & Bochmann, M. (1999). Advanced inorganic chemistry. John Wiley & Sons.
67. El-Boraey, H. A., & El-Din, A. A. S. (2014). Transition metal complex of a new 15-membered [N5] pentaazamacrocyclic ligand with their spectral and anticancer studies. Spectrochimica Acta Part A: Molecular and Biomolecular Spectroscopy, 132, 663–671.
68. Mosmann, T. (1983). Rapid colorimetric assay for cellular growth and survival: application to proliferation and cytotoxicity assays. Journal of Immunological Methods, 65(1–2), 55–63.